Monthly Notices
of the
ROYAL ASTRONOMICAL SOCIETY

Mon. Not. R. Astron. Soc. **406,** 43–59 (2010) doi:10.1111/j.1365-2966.2010.16481.x

# The redshift evolution of the mass function of cold gas in hierarchical galaxy formation models

C. Power,[1,2]★ C. M. Baugh[3] and C. G. Lacey[3]

[1]*Department of Physics & Astronomy, University of Leicester, Leicester LE1 7RH*
[2]*Centre for Astrophysics and Supercomputing, Swinburne University of Technology, PO Box 218, Hawthorn, 3122 Victoria, Australia*
[3]*Institute for Computational Cosmology, University of Durham, South Road, Durham DH1 3LE*

Accepted 2010 February 4. Received 2010 February 4; in original form 2009 July 27

**ABSTRACT**

Accurately predicting how the cosmic abundance of neutral hydrogen evolves with redshift is a challenging problem facing modellers of galaxy formation. We investigate the predictions of four currently favoured semi-analytical galaxy formation models applied to the Millennium simulation for the mass function of cold neutral gas (atomic and molecular) in galaxies as a function of redshift, and we use these predictions to construct number counts for the next generation of all-sky neutral atomic hydrogen (H I) surveys. Despite the different implementations of the physical ingredients of galaxy formation, we find that the model predictions are broadly consistent with one another; the key differences reflect how the models treat active galactic nuclei feedback and how the time-scale for star formation evolves with redshift. The models produce mass functions of cold gas in galaxies that are generally in good agreement with H I surveys at $z = 0$. Interestingly, we find that these mass functions do not evolve significantly with redshift. Adopting a simple conversion factor for cold gas mass to H I mass that we apply to all galaxies at all redshifts, we derive mass functions of H I in galaxies from the predicted mass functions of cold gas, which we use to predict the number counts of sources likely to be detected by H I surveys on next generation radio telescopes such as the Square Kilometre Array and its pathfinders. We find the number counts peak at $\sim 4 \times 10^3/4 \times 10^4/3 \times 10^5$ galaxies deg$^{-2}$ at $z \sim 0.1/0.2/0.5$ for a year long H I hemispheric survey on a 1/10/100 per cent SKA with a 30 deg$^2$ field of view, corresponding to an integration time of 12 h. On a full SKA with a 200 deg$^2$ field of view (equivalent to an integration time of 80 h) the number counts peak at $5 \times 10^5$ galaxies deg$^{-2}$ at $z \sim 0.6$. We show also how adopting a conversion factor for cold gas mass to H I mass that varies from galaxy to galaxy impacts on number counts. In addition, we examine how the typical angular sizes of galaxies vary with redshift. These decline strongly with increasing redshift at $z \lesssim 0.5$ and more gently at $z \gtrsim 0.5$; the median angular size varies between 5 and 10 arcsec at $z = 0.1$, 0.5 and 3 arcsec at $z = 1$ and 0.2 and 1 arcsec at $z = 3$ for galaxies with H I masses in excess of $10^9\, h^{-1}\, \mathrm{M}_\odot$, depending on the precise model. Taken together, these results make clear that the forthcoming H I surveys will provide important and powerful tests of theoretical galaxy formation models.

**Key words:** galaxies: formation – cosmology: theory – radio lines: galaxies.

## 1 INTRODUCTION

Neutral gas, predominantly atomic hydrogen (H I) along with molecular hydrogen ($H_2$) and helium (He), plays a fundamental role in galaxy formation, principally as the raw material from which stars are made. At any given time, the fraction of a galaxy's mass that is in the form of H I will be determined by the competing rates at which it is depleted (by e.g. star formation, photo-ionization and expulsion via winds) and replenished (by e.g. recombination and accretion from the galaxy's surroundings). These processes are integral to any theory of galaxy formation and so we expect that understanding how the H I properties of galaxies vary with redshift and environment will provide us with important insights into how galaxies form.

Our knowledge of H I in galaxies derives from radio observations of the rest frame 21 cm emission line, which allows us to measure the density, temperature and velocity distribution of H I

★E-mail: chris.power@astro.le.ac.uk

along our line of sight. Thanks to surveys such as H I Parkes All-Sky Survey (HIPASS; see Meyer et al. 2004) and more recently Arecibo Legacy Fast ALFA Survey (ALFALFA; see Giovanelli et al. 2005), we have a good understanding of the H I properties of galaxies in the low-redshift Universe, at $z \lesssim 0.05$. For example, HIPASS has revealed that most H I is associated with galaxies and that the galaxy population detected in 21 cm emission is essentially the same as that seen at optical and infrared wavelengths but weighted towards gas-rich systems, which tend to be late type (Meyer et al. 2004). Furthermore, HIPASS data have allowed accurate measurement of the local H I mass function of galaxies (the number density of galaxies with a given H I mass per unit comoving volume) and $\Omega_{\rm H\,I}$ (the global H I mass density in units of the present-day critical density $\rho_{\rm crit} = 3H_0^2/8\pi G$). Zwaan et al. (2005) found that the local H I mass function is well described by a Schechter function and they estimated the local cosmic H I mass density to be $\Omega_{\rm H\,I} = 3.5 \pm 0.4 \pm 0.4 \times 10^{-4}\, h_{75}^{-1}$ (with random and systematic uncertainties at the 68 per cent confidence limit), assuming a dimensionless Hubble parameter of $h_{75} = h/0.75 = 1$. This is approximately 1/10th the value of cosmic stellar mass density $\Omega_*$ at $z = 0$ (cf. Cole et al. 2001).

In contrast, we know comparatively little about H I in galaxies at higher redshifts (i.e. $z \gtrsim 0.05$). This is because detecting the rest frame 21 cm emission from individual galaxies has required too great a sensitivity for reasonable observing times.[1] There are estimates of $\Omega_{\rm H\,I}$ at high redshifts ($z \gtrsim 1.5$), but these have been deduced from quasi-stellar object absorption-line systems and imply that $\Omega_{\rm H\,I} \simeq 10^{-3}$ (e.g. Péroux et al. 2003; Prochaska, Herbert-Fort & Wolfe 2005; Rao, Turnshek & Nestor 2006). However, this situation will change dramatically over the next decade with the emergence of a series of next generation radio telescopes, culminating in the Square Kilometre Array (SKA) that is expected to see first light by about 2020. The SKA will have sufficient sensitivity and angular resolution to map H I in galaxies out to redshifts $z \gtrsim 3$ (see, for example Blake et al. 2004; Braun 2007). On a shorter time-scale a variety of SKA pathfinders such as the Australian SKA Pathfinder (ASKAP; see Johnston et al. 2008), the Karoo Array Telescope (MeerKAT; see Booth et al. 2009) and APERture Tile In Focus (APERTIF; see Verheijen et al. 2008) will carry out H I surveys that, in some cases, will probe the properties of galaxies out to $z \sim 1$.

Because we have so little data on H I in galaxies beyond the local Universe, the results of H I surveys on next generation radio telescopes will have a profound impact on our understanding of galaxy formation and evolution. For example, we have compelling evidence that the cosmic star formation rate density has decreased by an order of magnitude since $z \sim 1$ (Madau et al. 1996; Hopkins 2004), yet we know little about how the H I mass in galaxies evolved over the same period. This is precisely the kind of question we can hope to answer with forthcoming H I surveys. For this reason, it is both timely and important to take stock of what theoretical galaxy formation models tell us about how quantities such as $\Omega_{\rm H\,I}$ and the H I mass function vary with redshift and environment. Not only can such predictions help us to interpret the physical significance of observational data, they can also provide important input into the design of new radio telescopes.

The primary aim of this paper is to explore the predictions of currently favoured *semi-analytical* galaxy formation models (cf. Cole et al. 2000; Baugh 2006) for the properties of cold gas in galaxies as a function of redshift in a $\Lambda$ cold dark matter ($\Lambda$CDM) universe. In particular, we investigate the redshift variation of the cold gas mass function of galaxies and $\Omega_{\rm cold}$ (i.e. the cold gas mass density parameter) in the Millennium simulation (Springel et al. 2005). In addition, we convert the predicted cold gas masses to H I masses and we use the resulting H I mass functions, along with predictions for the radii and rotation speeds of galactic discs, to predict the number counts of sources one might expect to recover from H I surveys on a radio telescope with a collecting area of 1 / 10/100 per cent of the full SKA.

The secondary aim of this paper is to compare and contrast the predictions of four distinct galaxy formation models from the Durham and Munich groups. These models incorporate different treatments of the same physical processes and in some cases invoke distinct physical processes, for example, active galactic nuclei (AGN) heating versus supernova-driven super winds. Therefore, it is instructive to assess the robustness of the basic predictions and to examine whether or not these predictions are consistent between models. This addresses the criticism that semi-analytical galaxy formation models lack transparency and the uncertainty as to which predictions are robust and which are sensitive to modest changes in the model parameters. It is in this context that this work complements in a very natural way the study of Obreschkow et al. (2009a).

The layout of the paper is as follows. In Section 2, we present an overview of the four galaxy formation models we use in this study. In Section 3, we examine the basic predictions of these models for the evolution of the mass function and global mass density of cold gas between $0 \lesssim z \lesssim 2$, and we determine the relationship between cold gas mass and the circular velocities and scale radii of discs. Based on these predictions, in Section 4, we determine what the implications are for the number counts of H I sources in future H I surveys on next generation radio telescopes, discussing in some detail how we might convert from cold gas mass to H I mass in Section 4.1. Finally, in Section 5, we summarize our results and discuss how future H I surveys will provide a powerful test of theoretical models of galaxy formation.

## 2 GALAXY FORMATION MODELS

The evolution of the global cold gas density in the Universe and the cold gas content of galaxies depends upon the interplay between a number of processes:

(i) the rate at which gas cools radiatively within dark matter haloes;
(ii) the rate at which cold gas is accreted in galaxy mergers;
(iii) the rate at which cold gas is consumed in star formation;
(iv) the rate at which gas is reheated or expelled from galaxies by sources of feedback (e.g. photo-ionization, stellar winds, supernovae, AGN heating, etc.).

Semi-analytical modelling provides us with the means to study the balance between these phenomena in the context of a universe in which structure in the dark matter grows hierarchically (for a recent review, see Baugh 2006). The models refer to cold gas as gas that has cooled radiatively from a hot phase to below $10^4$ K and is available for star formation. The cold gas mass is predominately made up of

[1] Although in a handful of cases it has been possible to use a stacking technique to measure rest frame 21 cm emission by co-adding the signal from multiple galaxies using their observed optical positions and redshifts (see Zwaan 2000; Chengalur, Braun & Wieringa 2001; Lah et al. 2007, 2009).

neutral atomic hydrogen (H I), along with molecular hydrogen and helium (see discussion in Section 4.1).

Here, we consider four different semi-analytical galaxy formation models from the Durham and Munich groups. Although the models follow the same basic philosophy, the implementations of various processes differ substantially between the two groups. We also consider Durham models with different physical ingredients. To remove one possible source of difference between the models, all the models discussed here adopt the background cosmology used in the Millennium simulation ($\Omega_{\rm M} = 0.25$, $\Omega_\Lambda = 0.75$, $\Omega_{\rm b} = 0.045$, $\sigma_8 = 0.9$, $h = 0.73$; cf. Springel et al. 2005).

### 2.1 The models

We now list the different models considered in this paper, give their designation and a very brief description of the main features of each. The differences between the models are discussed in more detail later on in this section. The first three models are 'Durham' models, which use the GALFORM code and the fourth model is the current 'Munich' semi-analytical model. The model designations are those used in the Millennium archive[2] and in the subsequent plots.

(i) The Bower et al. (2006) model (hereafter Bower2006a). In this model, AGN heating suppresses the formation of bright, massive galaxies by stopping the cooling flow in their host dark matter haloes, thereby cutting off the supply of cold gas for star formation. This regulation of the cooling flow results in a sharp break at the bright end of the luminosity function. Bower2006a matches the evolution of the stellar mass function inferred from observations (e.g. Fontana et al. 2004; Drory et al. 2005), the number counts and redshift distribution of extremely red objects (Gonzalez-Perez et al. 2009) and the abundance of luminous red galaxies (Almeida et al. 2008).

(ii) The Font et al. (2008) model (hereafter Font2008a). This model extends Bower2006a with a fundamental change to the cooling model. Motivated by the simulations of McCarthy et al. (2008), which track the fate of the hot gas in haloes after their accretion by more massive objects, Font2008a assumes that the stripping of hot gas from satellite haloes is not completely efficient, contrary to the traditional recipe used in semi-analytical models. Instead, the satellite halo is assumed to retain some fraction of its hot gas, which is determined by its orbit within the larger halo. This gas can cool directly on to the satellite rather than the central galaxy in the halo. Font2008a gives an improved match to the proportions of red and blue galaxies seen in Sloan Digital Sky Survey (SDSS) groups (Weinmann et al. 2006a,b).

(iii) The Baugh et al. (2005) model (hereafter Baugh2005M). Baugh2005M matches the observed counts and redshifts of sub-mm galaxies and the luminosity function of Lyman-break galaxies, as well as observations of the local galaxy population, such as the sizes of galaxy discs (cf. Gonzalez et al. 2009) and cold gas mass fractions. In this model, merger-triggered starbursts make a similar contribution to the star formation rate per unit volume at high redshift to that from galactic discs. Starbursts are assumed to have a top-heavy stellar initial mass function (IMF), which Baugh et al. argued is essential for a hierarchical galaxy formation model to match the sub-mm counts, whilst at the same time reproducing observations of local galaxies. The formation of bright galaxies is regulated by a supernova-driven 'super winds', which expel gas from intermediate mass dark matter haloes (see Benson et al. 2003).

In this paper, we implement Baugh2005M in the Millennium simulation. The cosmology used in the Millennium simulation is somewhat different to that adopted in the original Baugh et al. model (the former has a matter density of $\Omega_{\rm M} = 0.25$, a dimensionless Hubble parameter of $h = 0.73$ and a power spectrum normalization of $\sigma_8 = 0.9$, whereas the latter used $\Omega_{\rm M} = 0.3$, $h = 0.7$ and $\sigma_8 = 0.93$). To reproduce the predictions of Baugh et al., we retain the baryon fraction $\Omega_{\rm b}/\Omega_{\rm m}$ of the original model, setting $\Omega_{\rm b} = 0.033$. The other galaxy formation parameters have *not* been changed. This model is not available in the Millennium archive.

(iv) The De Lucia & Blaizot (2007) model (hereafter DeLucia2006a). DeLucia2006a employs AGN feedback in the 'radio-mode' to restrict the formation of bright galaxies at the present day. This model is a development of those introduced by Croton et al. (2006) and De Lucia et al. (2006). It enjoys many of the same successes as Bower2006a, but, if anything, produces too many stars at high redshift (cf. Kitzbichler & White 2007).

### 2.2 Halo identification and merger trees

All of the models use halo merger histories extracted from the Millennium simulation, derived from identical group catalogues produced by the SUBFIND code of Springel et al. (2001). SUBFIND identifies distinct groups of particles using the 'friends-of-friends' (FOF) algorithm (cf. Davis et al. 1985) and then resolves each FOF group into self-bound overdensities. These self-bound overdensities correspond to subhaloes; the most massive subhalo within a FOF group is identified with the host dark matter halo while the remaining lower mass subhaloes within the group correspond to its substructures. There are as many group catalogues as there are output times and they are linked across multiple output times to produce merger trees.

Although the input group catalogues are identical, the Durham and Munich groups construct their merger trees independently using distinct algorithms. This means that it is possible to identify the same haloes at a given output time in the Durham and Munich models but the detailed merging histories of these haloes may differ. This difference reflects in part differences in the working definition of a halo. The Munich models track the set of particles that correspond to the most massive subhalo within the FOF group across output times (cf. Croton et al. 2006), whereas the Durham models track the set of particles that correspond, in general, to the FOF group (cf. Helly et al. 2003; Harker et al. 2006). In general, because these FOF groups are modified to avoid situations where the groups become prematurely or temporarily linked by bridges of low-density material (cf. Harker et al. 2006; Cole et al. 2008).

The difference also reflects how the host subhaloes of satellites are treated. In the Durham models, an infalling subhalo is considered a satellite galaxy of its more massive host halo once it loses in excess of 25 per cent of the mass it had at the time of its accretion and it lies within twice its host halo's half-mass radius (cf. Harker et al. 2006). Importantly, this subhalo is then treated as a satellite at all subsequent times, even if its orbit brings it outside of its host's virial radius at some later time. In contrast, the Munich models simply require that the infalling satellite lies within the virial radius of its host; if the subhalo's orbit takes it beyond the virial radius, it is no longer classed as a satellite (John Helly, private communication). Also, the Durham models require that the masses of subhaloes must increase *monotonically* with time, whereas the Munich models allow a subhalo's mass to either increase and decrease with time.

[2] The Millennium galaxy archive can be found at Durham (http://galaxy-catalogue.dur.ac.uk:8080/Millennium) or Munich (http://www.g-vo.org/Millennium).

Finally, the Durham models explicitly tag subhaloes that are satellites and treat them accordingly, whereas the Munich models do not treat subhaloes that host satellites any differently from subhaloes that do not.

### 2.3 Galaxy formation physics

We now highlight some of the areas in which there are either important differences in the implementation of the physics between the models or in which different processes have been adopted. For full descriptions of each model, we refer the reader to the original references given above. A comparison of Bower2006a and Baugh2005M is given in Almeida, Baugh & Lacey (2007); the differences between Bower2006a and Font2008a are set out in Font2008a.

(i) *Gas cooling: gas density and cooling radius*. The models all assume that gas cools primarily (for the haloes which typically host galaxies) by two-body collisional processes involving neutral or ionized atoms. The cooling rate depends upon the composition (metallicity) and the density of the gas. Gas is assumed to have cooled within some cooling radius, which is defined in different ways in the models. A further time-scale that regulates the addition of cold gas into a galactic disc is the free-fall time.

The models make different assumptions about the density profile of the gas and the cooling radius.

(a) DeLucia2006a assumes that the gas follows a singular isothermal profile (see Croton et al. 2006), and the cooling radius is defined as the radius at which the cooling time is equal to the dynamical time of the halo.

(b) Both Bower2006a and Font2008a assume that the hot gas density profile follows an isothermal profile with a constant density core, whose core radius is fixed and scales with the virial radius of the halo. The cooling radius propagates outwards as a function of time, reaching a maximum at the radius where the cooling time is equal to the lifetime of the dark matter halo (see Cole et al. 2000). In Font2008a, the cold gas yield is a factor of 2 higher than that adopted in Bower2006a, which gives a better match to observed galaxy colours (Gonzalez et al. 2009).

(c) Baugh2005M assumes that the hot gas follows an isothermal profile with a constant density core, whose core radius evolves with time as low-entropy gas cools (see Cole et al. 2000). The cooling radius is defined in the same way as in Bower2006a and Font2008a.

(ii) *Gas cooling: AGN heating of the hot halo.* Bower2006a, Font2008a and DeLucia2006a all modify the cooling flow in massive haloes by appealing to heating from radio-mode AGN feedback, following the accretion of material from the cooling flow on to a central supermassive black hole.

(iii) *Gas cooling: halo baryon fraction.* In Baugh2005M, there is no heating of the hot halo by AGN feedback. Instead, a new channel is introduced for gas heated by the energy released by supernova explosions. Some fraction of the gas, as is common in the majority of semi-analytical models, is reheated and re-incorporated, on some time-scale, into the hot gas halo (see Benson et al. 2003). The rest of the reheated gas is ejected from the halo altogether in the super wind. In the Baugh2005 model, this gas is not allowed to recool at any stage. This process becomes inefficient in more massive haloes. However, the cooling rate is reduced in such haloes because they have less than the universal fraction of baryons (due to super wind ejection of gas from their progenitors). A detailed description of how super winds are modelled in Baugh2005M is given in Lacey et al. (2008), who looked at the properties of galaxies in the infrared for comparison with observational data from the *Spitzer Space Telescope*.

(iv) *Gas cooling: cooling in satellites.* Font2008a introduced a new cooling scenario based on the hydrodynamical simulations of McCarthy et al. (2008). Traditionally, the ram-pressure stripping of the hot gas from a satellite halo has been assumed to be maximally efficient and instantaneous following a merger between two dark matter haloes. McCarthy et al. showed that in gas simulations this is not the case and that the satellite can retain a substantial amount of hot gas, with the fraction depending upon the satellite orbit. McCarthy et al. used a suite of simulations to calibrate a recipe to describe how much hot gas is kept. Font2008a extended the GALFORM code to include this prescription to calculate the amount of hot gas attached to each satellite galaxy within a halo and to allow the gas to cool directly on to the satellite, rather than on to the central (most massive) galaxy in the main dark matter halo. The other models considered in this paper do not allow gas to cool on to satellite galaxies.

(v) *Galaxy mergers.* Galaxies merge due to dynamical friction. Baugh2005M adopts the form of the merger time-scale given by equation (4.16) of Cole et al. (2000). Bower2006a and Font2008a use the same prescription with a time-scale that is longer by 50 per cent; physically, this can be explained as a reduction in the mass of the satellite halo due to tidal stripping. DeLucia2006a use a hybrid scheme in which a satellite galaxy is associated with a substructure halo, which is followed until stripping and disruption result in it dropping below the resolution limit of the simulation. From the last radius at which the substructure was seen, an analytic estimate of the merger time is made, using the dynamical friction time-scale (but with a different definition of the Coulomb logarithm) and applying a boost of a factor of 2 (to improve the match to the bright end of the present-day optical luminosity function).

(vi) *Star formation.* In the Durham models, the star formation time-scale scales according to circular velocity of the disc computed at the half-mass radius. The star formation time-scale also depends on a time-scale parameter which can be held fixed (Baugh2005M) or which can scale with the disc dynamical time (Bower2006a, Font2008a). All of the cold gas is available for star formation. In the Munich model (DeLucia2006a), a critical mass of cold gas has to be reached before star formation can begin. This is motivated by the observational inference that star formation requires a critical surface density of cold gas (which also has a theoretical motivation; cf. Kennicutt 1998). Only the cold gas mass in excess of the threshold is available for star formation. The time-scale adopted is the disc dynamical time. All the models adopt a standard solar neighbourhood IMF for quiescent star formation in discs, although Baugh2005M adopts a top-heavy IMF with a correspondingly higher yield and recycled fraction for episodes of star formation triggered by galaxy mergers.

(vii) *Heating of cooled gas by supernovae.* In the Durham models, the amount of gas reheated by supernova feedback per time-step is a multiple of the star formation rate, which depends principally on the circular velocity of the disc as well as the choice of values adopted for the feedback parameters. As we have touched upon in (3) above, in Baugh2005M, the gas reheated by supernovae can either be ejected completely in a super wind or heated up so that it is later re-incorporated into the hot halo (when a new halo forms i.e. after a doubling of the halo mass). Bower2006a and Font2008a do not consider the super wind channel for reheated gas. These models allow the reheated gas to be added to the hot gas reservoir on a time-scale which depends on the halo dynamical time, rather than waiting for a new halo to form. DeLucia2006a follows Croton

et al. (2006), who globally pins the rate at which gas is reheated by supernovae to a multiple of the star formation rate suggested by observations. The amount of energy released by supernovae is tracked and used to compute if any of the hot halo is ejected, to be re-incorporated on some time-scale.

A common feature of all the models presented in this paper is that they contain parameters that are set by requiring that the predictions reproduce a subset of the available observational data. The primary consideration when setting the model parameters is that the model reproduces the present-day optical luminosity function as closely as possible. However, this alone is insufficient to set all of parameters, and so selected secondary observations are matched in order to specify the model. For example, the observed gas fractions in spirals and the sizes of discs are used to determine the Baugh2005M parameters, while Bower2006a focuses on reproducing the bimodality of the colour distribution of local galaxies (cf. Gonzalez et al. 2009). In both cases, constraining the parameters in this way fixes the star formation time-scales in the models. We refer the reader to the original references for a more complete discussion of which data sets are reproduced by the respective models.

It is worth noting that, in the context of this study, gas fractions in spirals are the only data used to set parameters which explicitly relate to the cold gas content of galaxies;[3] other observations, such as the galaxy luminosity and mass functions, provide indirect constraints on the cold gas content. None of the model parameters have been adjusted for the purposes of this paper, except for the reduction in the cosmological baryon fraction in Baugh2005M, as explained above.

## 3 BASIC PREDICTIONS

In this section, we present the model predictions for the cold gas masses, radii and rotation speeds of galactic discs. These quantities are used in the next section to predict the 21 cm luminosity of the galaxies. Note that we do not discuss any quantities derived from these direct model outputs here, instead deferring such discussion until Section 4.

We begin by inspecting the cold gas mass functions predicted by the four models in Fig. 1 at $z = 0$ (upper panel) and $z = 1$ (lower panel). For comparison, we show also an 'observed' $z = 0$ cold gas mass function (open circles and error bars), obtained by converting the $z = 0$ mass function of H I in galaxies from HIPASS (cf. Zwaan et al. 2005) to a cold gas mass function, using the 'fixed $H_2$/H I ratio' conversion factor discussed in Section 4.1. The reader should note that cold gas masses are plotted in units of $h^{-2}\,M_\odot$ rather than $h^{-1}\,M_\odot$, which is the unit used in simulations. This ensures that the observational units (which depend upon the square of the luminosity distance) are matched, but it introduces an explicit dependence on the dimensionless Hubble parameter $h$; here, we adopt $h = 0.73$, the value used in the Millennium simulation.

We find that DeLucia2006a and Baugh2005M recover the observed $z = 0$ cold gas mass function reasonably well, following the data closely between $M_{\rm cold} \simeq 10^{8.5}\,h^{-1}\,M_\odot$ (approximately the cold gas mass resolution limit of the model; see below) and $M_{\rm cold} \simeq 10^{9.8}\,h^{-1}\,M_\odot$); at larger $M_{\rm cold}$, both models tend to overestimate the amount of cold gas in galaxies by ∼0.25 dex. In contrast, both Font2008a and Bower2006a predict systematically more cold gas in galaxies than is observed. This is unsurprising, however,

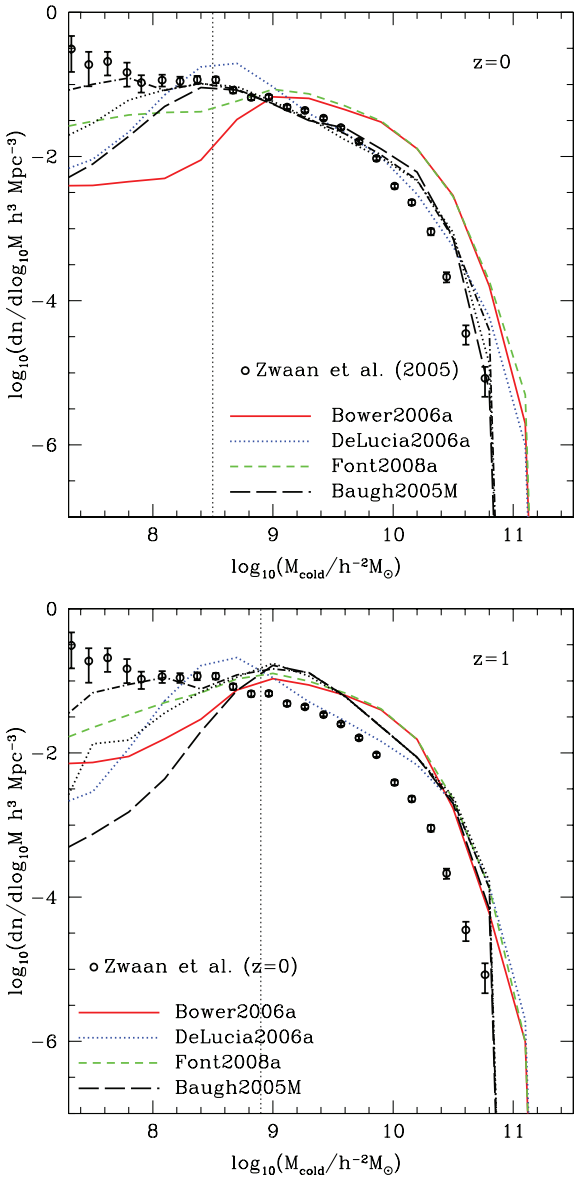


**Figure 1.** The predicted cold gas mass function at $z = 0$ (top) and $z = 1$ (bottom). The points show an observational estimate of the H I mass function at $z = 0$ by Zwaan et al. (2005), converted into a cold gas mass function by adopting the fixed $H_2$/H I ratio conversion factor described in Section 4.1. Different line types correspond to different models as indicated by the legend. For Baugh2005M, the results using the Millennium simulation merger trees are shown by the dashed black lines. The dotted and dot–dashed lines show calculations using Monte Carlo merger trees with improved mass resolution (with a mass resolution factor of 2 and 4 better than the Millennium simulation, respectively) but with the galaxy formation parameters held the same. The dotted vertical lines indicate the cold gas mass resolution limit of the Millennium galaxy formation models. The cold gas mass resolution limit is slightly higher at $z = 1$ than it is at $z = 0$. In the lower panel, the $z = 0$ data points are repeated for reference.

because both Font2008a and Bower2006a also overpredict the gas-to-stellar ratio in spirals (see the discussion in Cole et al. 2000 and their fig. 9).

There is a minimum mass below which haloes are not reliably resolved in the Millennium simulation and this in turn imposes a minimum cold gas mass below which the predictions of the galaxy formation models are unreliable. This arises because the simulation

[3] Even then, these data were used in only a subset of the models.

can only recover the abundance of dark matter haloes down to some limiting mass;[4] below this limiting mass, the abundance of low-mass haloes will be suppressed because of finite mass resolution of the simulation. Furthermore, low-mass haloes may not be sufficiently well resolved for their merger trees to be considered reliable; this mass is likely to be larger than required for convergence of the halo mass function.

This limiting halo mass is a problem because we expect cold gas to be present in haloes with masses below the resolution limit, and so we need to know how the limiting halo mass and the minimum cold gas mass relate to one another. This relationship can be estimated by running Monte Carlo merger trees of different minimum halo masses and comparing with the $N$-body merger trees. In practice, we run the Baugh2005M model with higher resolution trees generated using the new Monte Carlo prescription of Parkinson, Cole & Helly (2008) and determine the halo mass down to which the Monte Carlo merger trees give a good match to the trees extracted from the Millennium simulation. The cold gas mass functions calculated using the $N$-body trees and the Monte Carlo trees diverge below the mass indicated by the dotted vertical line in Fig. 1, at a cold gas mass of $M_{\rm cold} = 10^{8.5}\,h^{-1}\,{\rm M}_{\odot}$. Note that we should repeat this exercise for each model in principle because the resolution limit may be sensitive to the model recipes. However, given the close agreement between the predictions above this mass limit, we do not expect the variation in the cold gas mass resolution between models to be large and so we expect the limiting mass obtained with Baugh2005M to be a reasonable estimate for all the models.

We note that there is little evolution in the predicted mass functions back to $z = 1$. This is remarkable because it shows that the sources and sinks of cold gas more or less balance one another out. How can we understand this? We expect the sizes of galactic discs to decrease with increasing redshift. In three of the models (Bower2006a; DeLucia2006a; Font2008a) star formation proceeds on a time-scale that is proportional to the circular orbit time-scale in the disc, and so it follows that the star formation time-scale decreases with increasing redshift. However, gas cools from the hot halo on a time-scale that depends on local gas density; because density increases with increasing redshift, it follows that the cooling time-scale also decreases with increasing redshift. Therefore, we might expect that the amount of gas to cool per unit time will increase with the increasing redshift, but this is offset by the increasing numbers of stars that form per unit time with the increasing redshift. This leads competing sources (gas cooling) and sinks (star formation and mass ejection by winds) of cold gas to balance each other.

This explanation is compelling in its simplicity, but it is far from clear that it provides the complete picture of what is happening. Competition between sources and sinks of cold gas can plausibly balance each other, but it is worth noting that there is little evidence for evolution of the cold gas mass function in Baugh2005M, which rests on assumptions that are quite different from those of Bower2006a, DeLucia2006a and Font2008a. In particular, the star formation time-scale in Baugh2005M does not vary in proportion to the circular orbit time-scale in the disc, and so it is not obvious why the sources and sinks of cold gas should balance in this model, as they appear to. Understanding what physical processes drive the evolution of the cold gas mass function in the models is clearly an important issue, and one which shall be the focus of future work.

[4] Typically, this limiting mass is equivalent to ∼20 particles, required for the halo mass function to be converged (e.g. Jenkins et al. 2001).

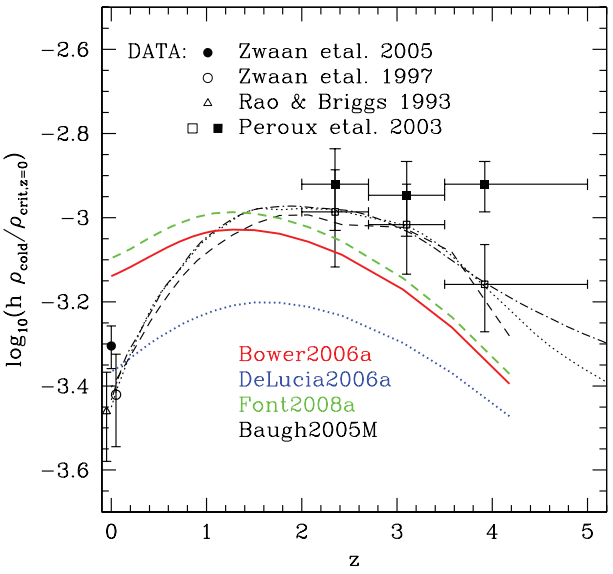


**Figure 2.** The predicted cold gas density $\rho_{\rm cold}$, normalized by the value of the critical density $\rho_{\rm crit}$ at $z = 0$, as a function of $z$. Different lines correspond to different models as indicated by the legend. For Baugh2005M, the results using the Millennium simulation merger trees are shown by the dashed black line. The dotted and dot–dashed lines show calculations using Monte Carlo merger trees with improved mass resolution but with the galaxy formation parameters held the same (see caption of Fig. 1). Filled and open circles correspond to Zwaan et al. (1997, 2005) data, respectively; open triangles correspond to Rao & Briggs (1993); open and filled squares correspond to Péroux et al. (2003). In the latter case, the open squares indicate the cold gas density inferred from damped Lyman $\alpha$ systems by Peroux et al., and the filled squares include a correction to take into account gas clouds with lower column density.

We now consider the global mass density of cold gas $\Omega_{\rm cold} = \rho_{\rm cold}/\rho_{\rm crit}$. In Fig. 2 we show how $\rho_{\rm cold}$ varies with redshift $z$, normalized by $\rho_{\rm crit}/h$ at $z = 0$ for ease of comparison with observational data. This reveals that both Bower2006a and Font2008a overpredict the density of cold gas at $z < 1$ and somewhat underpredict the amount of cold gas at higher redshifts. DeLucia2006a predicts a cold gas density that is consistent with observational estimates at $z = 0$, but it underpredicts the density at $z > 0$ by a factor of 2 to 3. Of all the models, Baugh2005M most closely matches the observed density of cold gas at all redshifts. Comparing the predictions for this model using the Millennium simulation merger trees with those from Monte Carlo merger trees (with improved mass resolution) suggests that the $N$-body results are robust up to $z \sim 4$.

We now compare the rotation speeds of galactic discs as a function of cold gas mass. This is interesting to quantify because it indicates how the velocity width is likely to scale with H I mass, which is important for H I surveys. It also provides a useful insight into how the mean cold gas mass varies as a function of galaxy mass, which can be related to the rotation speed.

Fig. 3 shows the rotation speed–cold gas mass relation for galactic discs at $z = 0$ (top) and $z = 1$ (bottom) predicted by the models. Note that the Durham and Munich models define rotation speed in different ways; in the Durham models, the rotation speed plotted is the circular velocity at the half-mass radius of the disc, whereas in the Munich model (DeLucia2006a), the rotation speed plotted is the circular velocity measured at the virial radius of the dark matter halo. The precise relationship between the circular velocities measured at the half-mass radius of the disc and at the virial radius of the host halo depends on the mass and distribution of the cold gas

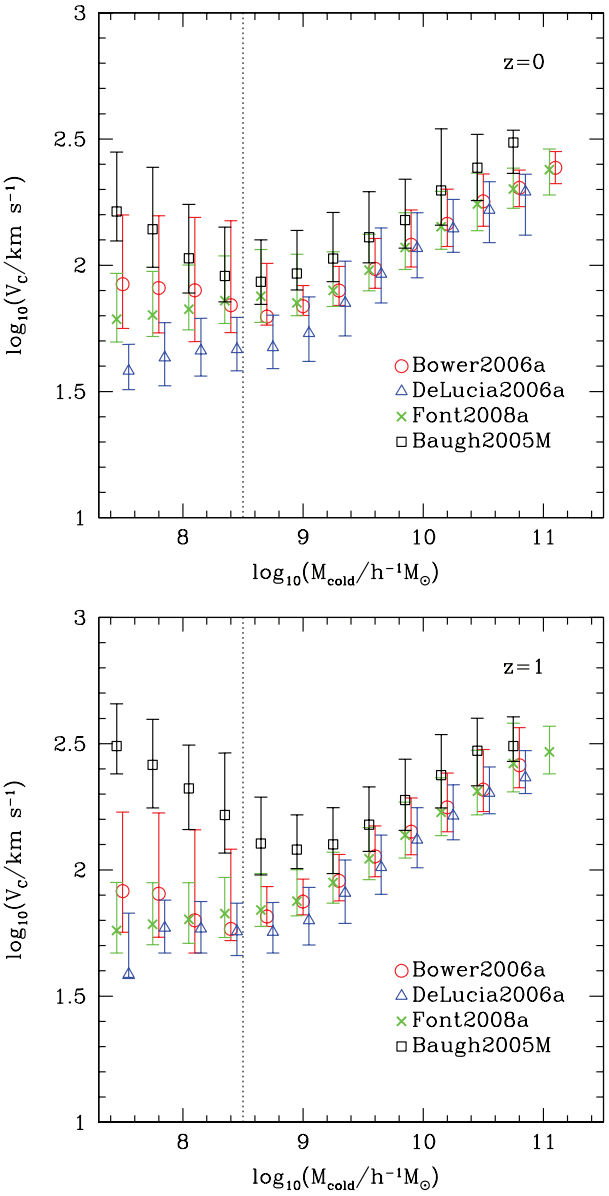


**Figure 3.** The predicted circular velocity–cold gas mass relation at $z = 0$ (top) and $z = 1$ (bottom). The points show the median velocity and the bars show the 10–90th percentile range. Different symbols correspond to different models as indicated by the legend. In DeLucia2006, the velocity plotted is measured at the virial radius of the dark matter halo; in the other cases, it is the circular velocity at the half-mass radius of the disc. The dotted vertical line indicates the cold gas mass resolution limit of the Millennium galaxy formation models.

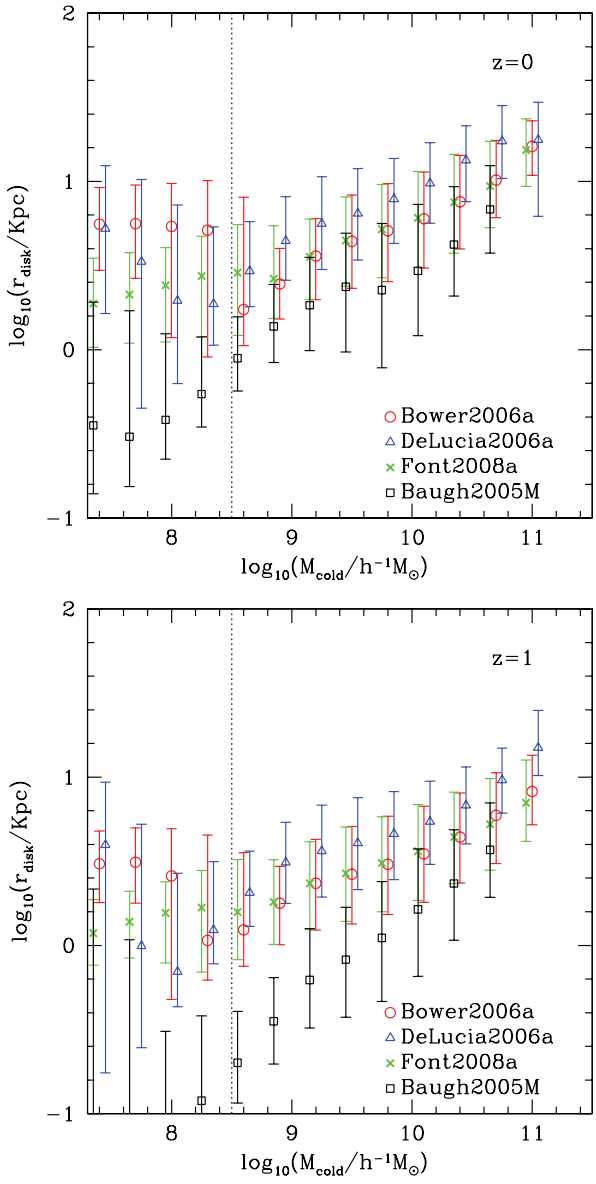


**Figure 4.** The predicted disc radius–cold gas mass relation at $z = 0$ (top) and $z = 1$ (bottom). The points show the median velocity and the bars show the 10–90th percentile range. Different symbols correspond to different models as indicated by the legend. The radius plotted is the half-mass radius of the disc. In DeLucia2006, the quantity stored in the Millennium archive is three times the scalelength of the exponential disc, which we convert to a half-mass radius. The dotted vertical line indicates the cold gas mass resolution limit of the Millennium galaxy formation models.

and stars in the disc and bulge and of the dark matter. For example, in Bower2006a, we find that the circular velocity at the half-mass radius of the disc is typically 20 per cent higher than that measured at the virial radius of the host halo, for $L^*$ galaxies. After allowing for this difference, the DeLucia2006a rotation speed–cold gas mass relation is in close agreement with the predictions of Bower2006a and Font2008a. This level of agreement is quite remarkable given the differences in the implementations of the physical ingredients in the models. In contrast, Baugh2005M predicts a rotation speed that is higher than the other models by around 50 per cent. One possible explanation for this is that discs are more compact in this model, which is indeed the case in Fig. 4 (see below).

The model predictions diverge from each other below a cold gas mass of $M_{\rm cold} = 10^{8.5}\,h^{-1}\,{\rm M}_{\odot}$ and there is a change in the slope of the rotation speed–cold gas mass relation below this mass. This is the minimum mass down to which the predictions from the Millennium simulation merger trees are reliable. There is very little evolution in the rotation speed–cold gas mass relation between $z = 0$ and 1; the zero-point of the $z = 1$ relation is about 25 per cent higher.

The predicted disc radius–cold gas mass relation is plotted in Fig. 4. For the Durham models, the disc radius plotted corresponds to the half-mass radius of the disc, which is calculated by taking into account conservation of the angular momentum of the cooling gas

and the dynamical equilibrium of the disc, bulge and dark matter.[5] For the Munich model (DeLucia2006a), the quantity stored in the Millennium archive is three times the scalelength of the exponential disc, which is computed by scaling from the virial radius of the dark matter halo. We convert this length to a half-mass disc radius to plot on Fig. 4.

The DeLucia2006a half-mass radii estimated in this way are approximately 0.2–0.3 dex larger than those predicted by Bower2006a and Font2008a. In contrast, Baugh2005M predicts smaller gas discs than the other models, but we note that this model also predicts sizes for stellar discs that are in much better agreement with observational data at $z = 0$ than the other models (Gonzalez et al. 2009). As with the rotation speed–cold gas mass relation, there is little evolution in the disc radius–cold gas mass relation between $z = 0$ and 1. The model predictions diverge from one another below the mass resolution of $M_{\rm cold} = 10^{8.5}\,h^{-1}\,{\rm M}_{\odot}$.

It is worth remarking that it is surprising that the DeLucia2006a, Bower2006a and Font2008a predictions are so close, given the differences in the way the disc sizes are computed in the models. One might expect the half-mass radii predicted by the Durham models to be smaller than those from the Munich model because the former take into account the gravitational contraction of the dark matter and the self-gravity of the disc and bulge, whereas the latter adopts a simple scaling of the virial radius of the host halo.

## 4 IMPLICATIONS FOR H I SURVEYS

The results presented so far encapsulate what current semi-analytical galaxy formation models can tell us about the distribution of cold gas masses of galaxies as a function of redshift. We can use this information to deduce the distribution of H I masses of galaxies, from which we can predict number counts of H I sources as a function of redshift. These predictions can then be compared with forthcoming H I surveys on the SKA pathfinders, such as ASKAP, MeerKAT and APERTIF, and ultimately on the SKA.

Such a comparison represents an important and fundamental test of the semi-analytical galaxy formation framework. Semi-analytical model parameters are calibrated explicitly to reproduce statistical properties of the observed galaxy population where observational data exist, such as the galaxy luminosity function (e.g. Benson et al. 2003) and the abundance of sub-mm galaxies at high redshift (Baugh2005M). However, this approach is sometimes criticized precisely because it is calibrated to reproduce properties of the observed galaxy population. It is not always clear how robust model predictions are if the parameters have been adjusted to match as many observational data sets as possible. Few observed data exist for the H I properties of galaxies at redshifts $z \gtrsim 0.05$, and so such data will provide a compelling test of the currently favoured models we consider in this paper.

In this section, we use the cold gas mass functions presented in the previous section to predict H I source number counts for forthcoming H I surveys. To do this, we must first convert cold gas masses, which are the natural outputs of the models, to H I masses. Then, we consider how the sensitivity and angular resolution of a radio telescope affects whether or not a particular galaxy at a given redshift is likely be detected in a given H I survey. Finally, we investigate the impact of sensitivity on the number counts of H I galaxies in 'peak flux limited' surveys and we assess the angular resolution required to resolve gas-rich galaxies out to $z \sim 3$.

### 4.1 Conversion of cold gas mass to H I mass

The results presented in Section 3 are for cold gas masses in galaxies, but we require H I masses. How should we convert from cold gas to H I mass?

(i) First, we note that ∼24 per cent by mass of this cold gas will be in the form of helium; this leaves ∼76 per cent by mass in the form of hydrogen.

(ii) Secondly, we note that this ∼76 per cent hydrogen will be split into neutral (atomic, molecular) and ionized fractions, but for simplicity we assume that the ionized fraction in the disc is sufficiently small that we can ignore it.

(iii) Thirdly, we must determine what fraction of the neutral hydrogen is molecular in form; this then allows us to assign an H I mass to each galaxy, given its cold gas mass.

It is worth providing some justification for our argument that the ionized fraction is small. Recall that we consider cold gas to be gas that has cooled radiatively from a hot phase to below $10^4$ K and is available for star formation (cf. Section 2). At a temperature of $\lesssim 10^4$ K, this cold gas will include warm hydrogen in its atomic and ionized phases (cf. Ferrière 2001). Observations tell us that the ratio of ionized to atomic hydrogen in the midplane of the Galaxy is small (∼5 per cent) but it increases with increasing scaleheight, and by scaleheights $\gtrsim 1$ kpc the warm ionized state probably dominates (cf. Reynolds 2004). The typical (i.e. full width at half-maximum) scaleheights of atomic and molecular hydrogen are much smaller than this (∼100–200 pc), and so what one estimates for the ionized mass within the disc depends on the range of scaleheights included. We adopt the mass estimates of Ferrière (2001) for the total ionized and neutral hydrogen masses of the Galaxy ($\gtrsim 7.5 \times 10^9$ and $\gtrsim 1.6 \times 10^9\,{\rm M}_{\odot}$) to estimate that the ionized fraction constitutes approximately 15 per cent by mass of the Galactic disc. This is sufficiently small that we can ignore it for the purposes of this study, although more detailed modelling would need to take it into account.

Of the remaining ∼76 per cent by mass of cold gas that is in the form of neutral hydrogen, what is the ratio of molecular ($H_2$) to atomic (H I) hydrogen? We consider two approaches:

(i) a 'fixed $H_2$/H I' ratio for all galaxies for all redshifts (cf. Baugh et al. 2004);

(ii) a 'variable $H_2$/H I' ratio that depends on galaxy properties and redshift (cf. Obreschkow & Rawlings 2009; Obreschkow et al. 2009b).

The fixed $H_2$/H I approach was used in the Baugh et al. (2004) study and it allows us to apply a simple uniform scaling to the cold gas mass functions presented in Section 3 to obtain H I mass functions. It is a purely empirical scaling in the sense that it uses estimates of the global $H_2$ and H I densities in the local Universe to deduce the ratio of molecular to atomic hydrogen. Baugh et al. (2004) used the estimates of Keres, Yun & Young (2003) and Zwaan et al. (2005), respectively, for the global $H_2$ and H I densities [$\rho_{\rm H_2} = (3.1 \pm 0.9) \times 10^7 h\,{\rm M}_{\odot}\,{\rm Mpc}^{-3}$ and $\rho_{\rm HI} = (8.1 \pm 1.3) \times 10^7 h\,{\rm M}_{\odot}{\rm Mpc}^{-3}$] to deduce a ratio of molecular to atomic hydrogen of ∼0.4. This gives a conversion factor of

$$M_{\rm HI} = 0.76\,M_{\rm cold}/(1 + 0.4) \simeq 0.54\,M_{\rm cold}, \quad (1)$$

which is the one we adopt.

[5] See Cole et al. (2000), Almeida et al. (2007) and Gonzalez et al. (2009) for details of this calculation.

The variable $H_2/H\,I$ approach is based on the work of Blitz & Rosolowsky (2006), Leroy et al. (2008) and Obreschkow et al. (2009a), and it allows us to estimate the $H_2/H\,I$ ratio on a galaxy-by-galaxy basis. There have been various attempts to predict theoretically the variation of the $H_2/H\,I$ ratio on galactic scales based on physical models of the ISM; for example, Elmegreen (1993) argued that the most important physical parameters driving variations in the $H_2/H\,I$ ratio are the gas pressure and the local intensity of the interstellar UV radiation field, while Krumholz, McKee & Tumlinson (2009) argued instead that the main physical parameters driving variations are the column density and metallicity of interstellar gas clouds. On the other hand, Wong & Blitz (2002) found from spatially resolved observations of nearby galaxies that the ratio of $H_2$ to H I surface densities increases with increasing midplane hydrostatic gas pressure, following a power-law relation $\Sigma_{H_2}/\Sigma_{H\,I} \propto P_0^{\alpha}$. This empirical power-law relation was then confirmed in more detailed observational studies by Blitz & Rosolowsky (2006) and Leroy et al. (2008), and found to extend from $\Sigma_{H_2}/\Sigma_{H\,I} \ll 1$ to $\Sigma_{H_2}/\Sigma_{H\,I} \gg 1$. Note that the midplane pressure $P_0$ used in these relations is not directly measured, but is instead inferred from the gas and stellar surface densities combined with assumed velocity dispersions or scaleheights, assuming hydrostatic equilibrium.

Building on this work, Obreschkow et al. (2009a) have derived a model for the global $H_2/H\,I$ ratio in a galaxy. This uses the $\Sigma_{H_2}/\Sigma_{H\,I} = (P_0/P_*)^{\alpha}$ relation in the form found by Leroy et al. (2008), with $\alpha = 0.8$ and $P_* = 2.35 \times 10^{-13}$ Pa, and assumes that the stars and gas in a galactic disc both have exponential profiles, though with different radial scalelengths. After setting the free parameters of the model by comparison with observational data on nearby galaxies, Obreschkow et al. obtain the following expression for the global $H_2/H\,I$ ratio, $R_{mol}^{gal} = M_{H_2}/M_{H\,I}$:

$$R_{mol}^{gal} = \left(3.44\, {R_{mol}^{c}}^{-0.506} + 4.82\, {R_{mol}^{c}}^{-1.054}\right)^{-1}, \quad (2)$$

where $R_{mol}^{c}$ is the $H_2/H\,I$ ratio at the centre of the disc, given by

$$R_{mol}^{c} = \left[K r_{disc}^{-4}\, M_{gas}\left(M_{gas} + \langle f_\sigma \rangle\, M_{disc}^{*}\right)\right]^{0.8}. \quad (3)$$

In the above expressions, $M_{disc}^{*}$ and $M_{gas}$ are the masses of stars and gas in the disc, and $r_{disc}$ is the exponential scalelength of the gas, while $K = G/(8\pi P_*) = 11.3\,m^4\,kg^{-2}$, $\langle f_\sigma \rangle = 0.4$ is the average ratio of the vertical velocity dispersions of gas to stars. Given $R_{mol}^{gal}$, the conversion factor between cold gas mass and H I mass is then

$$M_{H\,I} = 0.76\, M_{cold} \Big/ \left(1 + R_{mol}^{gal}\right). \quad (4)$$

We employ equations (2)–(4) using the values of $M_{disc}^{*}$ and $M_{gas}$ predicted by the semi-analytical models. Because neither the Durham nor Munich models distinguish between the half-mass radii of the stars and gas, we take the gas half-mass radius to be equal to the total half-mass radius predicted by the semi-analytical model, and we then convert it to a disc scalelength $r_{disc}$ by assuming an exponential disc (as in Obreschkow et al.).

How significant is the difference between the H I masses estimated assuming a variable $H_2/H\,I$ approach and those estimated assuming a fixed $H_2/H\,I$ approach? Fig. 5 shows the distribution of the ratio $M_{H_2}/M_{H\,I}$ (i.e. $R_{mol}^{gal}$) for galaxies at $z = 0$ in Bower2006a. This is interesting because $R_{mol}^{gal}$ fixes $M_{H\,I}$ for a galaxy, given $M_{cold}$ (cf. equation 4), and so knowledge of the distribution of $R_{mol}^{gal}$ provides important information about the distribution of $M_{H\,I}$. We split our galaxy sample by $M_{cold}$ into three mass bins, of width 0.3 dex, centred on $M_{cold} = 10^9, 10^{9.5}$ and $10^{10}\,M_\odot$ (solid, dotted and dashed histograms); these contain 55 042, 60 579 and 32 213 galaxies, respectively. For each mass bin, we construct a histogram of $M_{H_2}/M_{H\,I}$ estimated using equation (2) and we normalize it by the area under the curve. For comparison, we indicate also the ratio $M_{H_2}/M_{H\,I}$ one obtains assuming a fixed $H_2/H\,I$ approach by the light dotted vertical line.

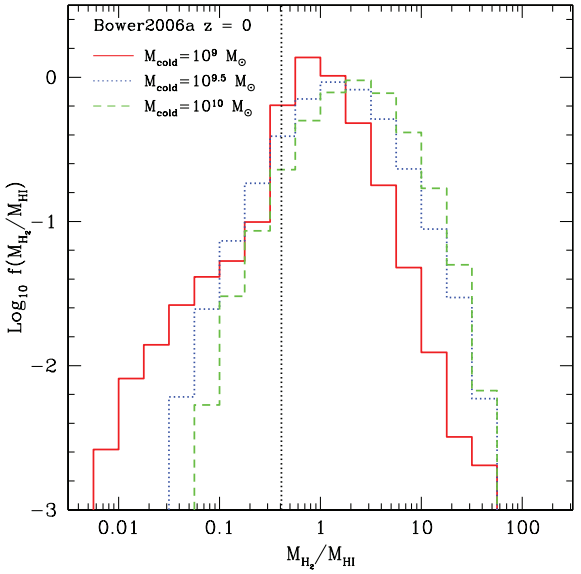


**Figure 5.** Distribution of the ratio $M_{H_2}/M_{H\,I}$ ($R_{mol}^{gal}$) predicted by the variable $H_2/H\,I$ approach for galaxies with cold gas masses $M_{cold} = 10^9/10^{9.5}/10^{10}\,M_\odot$ (solid, dotted and dashed histograms, respectively) in Bower2006a at $z = 0$. We include all galaxies within a bin of 0.3 dex centred on $M_{cold}$. The histograms are normalized by the area under the curve. The light dotted vertical line indicates the ratio assumed if the fixed $H_2/H\,I$ approach is used.

Fig. 5 is striking because it shows that variable $H_2/H\,I$ approach predicts a broad distribution of $M_{H_2}/M_{H\,I}$ in each mass bin. The medians of the distributions are ∼0.9, ∼1.5 and ∼2.2 in the bins centred on $M_{cold} = (10^9/10^{9.5}/10^{10})\,M_\odot$, compared to ∼0.4 assumed in the fixed $H_2/H\,I$ approach; indeed, only ∼11 per cent of the galaxies in the $M_{cold} = 10^9/10^{9.5}\,M_\odot$ mass bins and ∼5 per cent in the $M_{cold} = 10^9\,M_\odot$ mass bin have $M_{H_2}/M_{H\,I}$ ratios as small as this. Physically, this means that a typical galaxy will have a smaller fraction of its cold gas mass in the form of H I – by as much as a factor of ∼100 – in the variable $H_2/H\,I$ approach than in the fixed $H_2/H\,I$ approach. Inspection of equation 3 suggests that this behaviour reflects the strong scaling with $r_{disc}$ ($\propto r_{disc}^4$). Within a given mass bin, there is a distribution of $r_{disc}$ and the 10th and 90th percentiles of this distribution differ by a factor of at least a few with respect to the median, translating into variations of factors of ∼20–100 in surface density and consequently local gas pressure with respect to the median. This implies that the $M_{H_2}/M_{H\,I}$ ratio can in principle vary by factors of $\sim 10^2$ to $10^4$ within a given mass bin, which will affect the number of H I sources that can be detected.

The dependence on $r_{disc}$ in the variable $H_2/H\,I$ approach implies that the mean/median $M_{H_2}/M_{H\,I}$ ratio should increase sharply with increasing redshift, which in turn implies that H I masses of galaxies should be smaller at high redshifts. This is made clear in Fig. 6 , which shows how the median of the distribution of $M_{H_2}/M_{H\,I}$ for all galaxies with $M_{cold} \geq 10^{8.5}\,M_\odot$ varies with redshift for the four models. In all cases, the median increases with redshift, as we would expect. However, the most striking aspect of this figure is the pronounced offsets between different models. The DeLucia2006a medians are an order of magnitude smaller than the Bower2006a/Font2008a medians at all redshifts. In contrast,

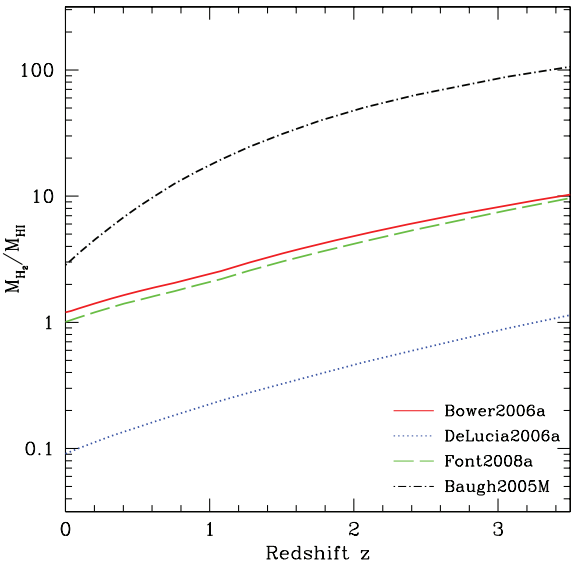


**Figure 6.** Variation of the median $M_{\rm H_2}/M_{\rm H\,I}$ (i.e. $R_{\rm mol}^{\rm gal}$) of all galaxies with $M_{\rm cold} \geq 10^{8.5}\,{\rm M}_{\odot}$ with redshift. Different lines correspond to different models as indicated by the legend.

Baugh2005M predicts a median that is a factor of a few larger at $z = 0$ than the Bower2006a/Font2008a medians, but the difference grows to a factor of $\sim$10 by $z \sim 3$. The models predict broadly similar cold gas and stellar masses and so it is the differences in scalelengths, apparent in Fig. 4, and the strong scaling with disc scalelength ($\propto r_{\rm disc}^4$) that drive these large offsets. The net effect of this strong variation of $M_{\rm H_2}/M_{\rm H\,I}$ with redshift will be to dramatically reduce the number of H I sources detectable at higher redshift (see Fig. 8 in the next section).

This demonstrates that how one chooses to calculate a galaxy's H I mass is important. However, for the purposes of this study, we adopt the fixed $\rm H_2/H\,I$ approach to converting cold gas masses to H I masses. The variable $\rm H_2/H\,I$ approach has been calibrated using observations of galaxies in the local Universe. There are sound physical reasons to expect that there will be a correlation between local gas pressure and molecular fraction in galactic discs at all redshifts, but it is unclear how reliable the local correlation is likely to be when applied to high redshifts. In contrast, the fixed $\rm H_2/H\,I$ approach provides a reasonable upper bound to the number of sources we might expect to detect.

### 4.2 Detection of H I sources

Two issues are key in determining whether or not an H I source will be detected reliably by a radio telescope or interferometer; namely, sensitivity and angular resolution. An H I source has an intrinsic 21 cm luminosity that depends primarily on its H I mass $M_{\rm H\,I}$ which, along with its line-of-sight velocity width $\Delta V_{\rm los}$ and distance $D$, determines the flux at the position of the observer. The observer measures this flux with a receiver that has finite sensitivity determined primarily by its effective collecting area $A_{\rm eff}$ and the system temperature $T_{\rm sys}$, and it is this limiting sensitivity that determines whether or not the source is detected. Note, however, that angular resolution also plays an important role; H I 21 cm emission from a galaxy is likely to be spatially extended and an extended source can be 'resolved out' by an interferometer if it is observed with too high an angular resolution. In the next two sections, we consider how sensitivity and angular resolution affect H I source number counts.

#### 4.2.1 Sensitivity

If we could construct the ideal radio telescope with arbitrarily high sensitivity, then we would observe a flux $S_{\rm obs}$ from an H I source at redshift $z$. This is determined by the source's H I mass $M_{\rm H\,I}$, its velocity width $\Delta V_{\rm los}$ and redshift $z$. The relationship between $S_{\rm obs}$ and $M_{\rm H\,I}$, $\Delta V_{\rm los}$ and $z$ can be obtained as follows.

The emissivity $\epsilon_{\nu_0}$ at rest-frame frequency $\nu_0$ tells us the rate at which energy is emitted by an H I source at this frequency per unit volume per steradian. We can express this as

$$\epsilon_{\nu_0} = \frac{1}{4\pi} h\nu_0 A_{12} \frac{n_2}{n_{\rm H}} n_{\rm H} \phi(\nu_0), \tag{5}$$

where $h\nu_0$ is the energy of the 21 cm photon ($h$ is the Planck constant and $\nu_0$ is the photon frequency), $n_2/n_{\rm H}$ tells us what fraction of atoms are expected to be in the upper state, $A_{12}$ is the Einstein coefficient which tells us the spontaneous rate of the transition from the upper to lower state, $n_{\rm H}$ is the total number density of hydrogen atoms in the source and $\phi(\nu)$ is the line profile. We expect $n_2/n_{\rm H} \simeq 3/4$ because the temperature of the cloud corresponds to a much larger energy than the energy difference corresponding to the transition from the upper to lower state (i.e. $kT \gg h\nu$, cf. Spitzer 1978). Integrating over a solid angle of $4\pi$ steradians and over the volume of the source gives us the luminosity at frequency $\nu_0$, $L_{\nu_0}$,

$$L_{\nu_0} = \frac{3}{4} h\nu_0 A_{12} \frac{M_{\rm H\,I}}{m_{\rm H}} \phi(\nu_0), \tag{6}$$

where we write the number of hydrogen atoms as $M_{\rm H\,I}/m_{\rm H}$, $m_{\rm H}$ being the mass of the hydrogen atom.

When we observe 21 cm emission from an H I source, the radiation arises from a forbidden transition, which implies a small natural line width ($5 \times 10^{16}$ Hz). Therefore, the observed line profile $\phi(\nu_0)$ is in practice determined by Doppler broadening due to the motions of H I atoms in the galaxy, which, in disc galaxies, are dominated by the large-scale rotational velocity. We therefore assume that $\phi(\nu_0)$ can be approximated as a top hat function of width $\Delta\nu_0 = (\Delta V_{\rm los}/c)\nu_0$ and height $1/\Delta\nu_0$. Noting this, we can write the total monochromatic flux at the position of the observer as

$$S_\nu = (1+z)\frac{L_{\nu(1+z)}}{4\pi D_{\rm L}(z)^2}; \tag{7}$$

here, $\nu = \nu_0\,(1+z)^{-1}$ is the redshifted frequency measured by the observer and $D_{\rm L}(z) = (1+z)\,D_{\rm co}(z)$ is the luminosity distance of the source with respect to the observer [$D_{\rm co}(z)$ is the radial comoving separation between source and observer]. Therefore, the measured flux at the position of the observer is

$$S_{\rm obs}\,\Delta\nu = \frac{3}{16\pi}\frac{h\nu A_{12}}{m_{\rm H}} M_{\rm H\,I} \frac{1}{D_L(z)^2}(1+z), \tag{8}$$

which we rewrite as

$$S_{\rm obs} = \frac{3}{16\pi}\frac{hcA_{12}}{m_{\rm H}} M_{\rm H\,I} \frac{1}{D_L(z)^2}\frac{1}{\Delta V_{\rm los}}(1+z). \tag{9}$$

Here, we assume that $\Delta\nu$ in equation (8) can be written as

$$\Delta\nu = \frac{\Delta\nu_0}{1+z} = \frac{\Delta V_{\rm los}}{c}\frac{\nu_0}{1+z}, \tag{10}$$

where $\Delta V_{\rm los}$ is the rest-frame line-of-sight velocity width of the galaxy. $\Delta V_{\rm los}$ will depend on the inclination $i$ of the disc, varying as $2\,V_{\rm c}\sin i$ where $V_{\rm c}$ is the disc circular velocity, and $i = 0$ or $\pi/2$ correspond to a face-on or edge-on disc, respectively. In our analysis, we assume that galaxy discs have random inclinations with respect to the observer, with an average velocity width of $\sim$1.57 $V_{\rm c}$ (cf. Section 4.3).

The measured flux from the source must be compared with the intrinsic limiting sensitivity of the receiver. Assuming a dual polarization radio receiver, the limiting rms flux $S_{\rm rms}$ can be calculated in a straightforward manner (cf. Burke & Graham-Smith 1996):

$$S_{\rm rms} = \frac{2\,k_{\rm B}\,T_{\rm sys}}{A_{\rm eff}\sqrt{2\,\Delta\nu_{\rm rec}\,\tau}}, \quad (11)$$

where $A_{\rm eff}$ is the total (effective) collecting area of the telescope, $T_{\rm sys}$ is the system temperature, $\Delta\nu_{\rm rec}$ is the bandwidth used in the receiver, $\tau$ is the integration time and $k_{\rm B}$ is Boltzmann's constant. The effective area $A_{\rm eff}$ and system temperature $T_{\rm sys}$ are the key parameters. The SKA will have an effective area[6] of the order of $A_{\rm eff} = 1$ km$^2$ and its pathfinders will have effective areas of a percentage of this; for pathfinders such as ASKAP, MeerKAT and APERTIF, this percentage will be $\lesssim$1 per cent. A conservative estimate of the system temperature would be $T_{\rm sys} = 50$ K. We can rewrite equation (11) as

$$\frac{S_{\rm rms}}{1.626\,\mu{\rm Jy}} = \left(\frac{A_{\rm eff}}{{\rm km}^2}\right)^{-1}\left(\frac{T_{\rm sys}}{50\,{\rm K}}\right)\left(\frac{\Delta\nu_{\rm rec}}{\rm MHz}\right)^{-1/2}\left(\frac{\tau}{\rm h}\right)^{-1/2}, \quad (12)$$

where $1\,{\rm Jy} = 10^{-26}\,{\rm W\,m^{-2}\,Hz^{-1}}$. The limiting flux sensitivity of the telescope $S_{\rm lim}$ is then $S_{\rm lim} = n_\sigma\,S_{\rm rms}$, where $n_\sigma$ defines the threshold for a galaxy to be reliably detected. Once we have fixed the integration time $\tau$ and the bandwidth $\Delta\nu_{\rm rec}$, we have the limiting sensitivity of our radio telescope.

It is worth remarking on the relationship between the frequency bandwidth $\Delta\nu_{\rm rec}$ in equations (11) and (12), which is particular to the radio telescope, and the frequency width $\Delta\nu$ in equations (8) and (9), which is set by the velocity width of the H I line $\Delta\,V_{\rm los}$. If we are to maximize the signal-to-noise ratio for detecting the galaxy in a survey, then it is important that these bandwidths are matched. The overall telescope frequency bandwidth at a given frequency will be broad – typically $\gtrsim$100 MHz – and much greater than the velocity width of an individual galaxy (e.g. $\sim$1 MHz corresponds to a $\sim$200 km s$^{-1}$ galaxy), but the overall bandwidth consists of $\sim 10^3$ to $10^4$ frequency channels that are much narrower than the expected frequency width of a galaxy. Therefore, a single telescope pointing will produce a huge data cube centred on a frequency $\nu$ with an overall bandwidth that consists of thousands of narrower frequency channels $\delta\nu$. These channels will then be rebinned to produce data cubes with different frequency resolutions $\Delta\nu_{\rm rec}$, and one of these rebinnings will have $\Delta\nu_{\rm rec} \simeq \Delta\nu$, which will be optimal for detecting an individual galaxy of a given velocity width with a sufficiently high signal-to-noise ratio.

#### 4.2.2 *Angular resolution*

The angular resolution of the radio telescope becomes important when the H I source is extended rather than a point source. For a single dish telescope, the angular resolution is $\sim\lambda/D$, where $\lambda$ is the wavelength of the radiation and $D$ is the diameter of the dish. Sources with angular sizes $\theta$ smaller than this are indistinguishable from point sources. For radio interferometers, it is the lengths of the baselines between pairs of dishes $B$ rather than the diameters of individual dishes that dictate the angular resolution. If the longest baseline is $B_{\rm max}$ and the shortest is $B_{\rm min}$, then the interferometer will resolve angular scales roughly from $\Theta_{\rm min} = \lambda/B_{\rm max}$ to $\Theta_{\rm max} = \lambda/B_{\rm min}$. Interferometers can therefore provide higher angular resolution than a single dish, which is desirable because it allows for H I sources to be mapped in greater detail. However, sources more extended than $\sim\Theta_{\rm max}$ get resolved out, and have their fluxes underestimated. The fraction of a galaxy's flux that is resolved out will depend on, for example, the precise distribution of interferometer baselines and what one assumes for the surface brightness profile of the galaxy (see e.g. the discussion in Abdalla, Blake & Rawlings 2010). In the case of the SKA, the shortest baseline is expected to be 20 m, which corresponds to an angular resolution of $\Theta_{\rm max} \sim 2100$ arcsec at $\lambda = 21$ cm, while the maximum baseline will be $\gtrsim$3000 km, which corresponds to a resolution $\Theta_{\rm min} \sim 0.1$ arcsec. As we will see in Section 4.3, the predicted H I sizes of galaxies in cosmological surveys are typically of the order of arcseconds or smaller, so there should not be any problem in practice with galaxies being resolved out.

### 4.3 Predictions for observables

First, we examine the predictions of the four models for the number counts ${\rm d}N/{\rm d}z$ of H I galaxies per square degree of sky as a function of redshift. By number counts, we mean the number of H I sources ${\rm d}N$ that can be detected in a redshift interval ${\rm d}z$ centred on a redshift $z$:

$$\frac{{\rm d}N}{{\rm d}z} = \frac{{\rm d}V}{{\rm d}z}\int_0^\infty \frac{{\rm d}n}{{\rm d}M}\,f(M)\,{\rm d}M, \quad (13)$$

where ${\rm d}V/{\rm d}z$ is the cosmological volume element at redshift $z$, ${\rm d}n/{\rm d}M$ is the H I mass function at $z$ and $f(M)$ represents the fraction of galaxies with H I mass $M$ that can be detected by the radio telescope. For simplicity, we assume that $f(M)$ depends only on limiting sensitivity, which depends on $M_{\rm H\,I}$. The angular resolution of the telescope also plays a role but its influence on $f(M)$ requires further assumptions to be made about, for example, the distribution of baselines, the clumpiness of H I within galaxy, its surface density profile, etc. and so we ignore this dependence.

In estimating predicted number counts, we assume a peak flux limited survey lasting 1 yr on a radio telescope with an effective area $A_{\rm eff}$ of 1, 10 and 100 per cent of the fiducial SKA.[7] We make the simplifying assumption that the field of view is fixed with redshift and consider two cases – 200 deg$^2$, which could be achieved on the SKA (cf. Taylor 2008), and 30 deg$^2$, which is expected on ASKAP (cf. Johnston et al. 2008). Assuming that the survey covers a complete hemisphere (i.e. $2\pi$ sr), this gives effective integration times on a patch of sky of $\tau = 80$ and 12 h, respectively. The measured flux $S_{\rm obs}$ from a galaxy is estimated using equation (9). The velocity width $\Delta V_{\rm los}$ is taken to be $2V_{\rm c,half}\sin i$, where $V_{\rm c,half}$ is the circular velocity at the half-mass radius of the galaxy. Galaxies are given random inclinations $i$, drawn from a uniform distribution in $\cos i$. The measured flux is compared to the limiting flux $S_{\rm rms}$ (equation 11) on a galaxy-by-galaxy basis [assuming $\Delta\nu_{\rm rec} = \Delta\nu$ and using equation (10) to estimate $\Delta\nu$] to estimate the signal-to-noise ratio. Our criterion for detection is $S_{\rm obs}/S_{\rm rms} \geq n_\sigma = 10$.

Fig. 7 shows how the number counts of H I galaxies varies with redshift for surveys with $A_{\rm eff}$ of 100 per cent (top left-hand panel for an integration of 80 h, top right-hand panel for an integration time of 12 h), 10 per cent (bottom left-hand panel) and 1 per cent (bottom right-hand panel) the effective area of the fiducial SKA

[6] Despite its name, it is unlikely that the SKA will have an area of 1 km$^2$; instead, it is likely to be $\sim$0.5 km$^2$, which ensures greater survey speed at the expense of sensitivity.

[7] Assuming that the SKA has an effective area of 1 km$^2$, although as noted already, the final SKA is likely to have an effective area smaller than this.

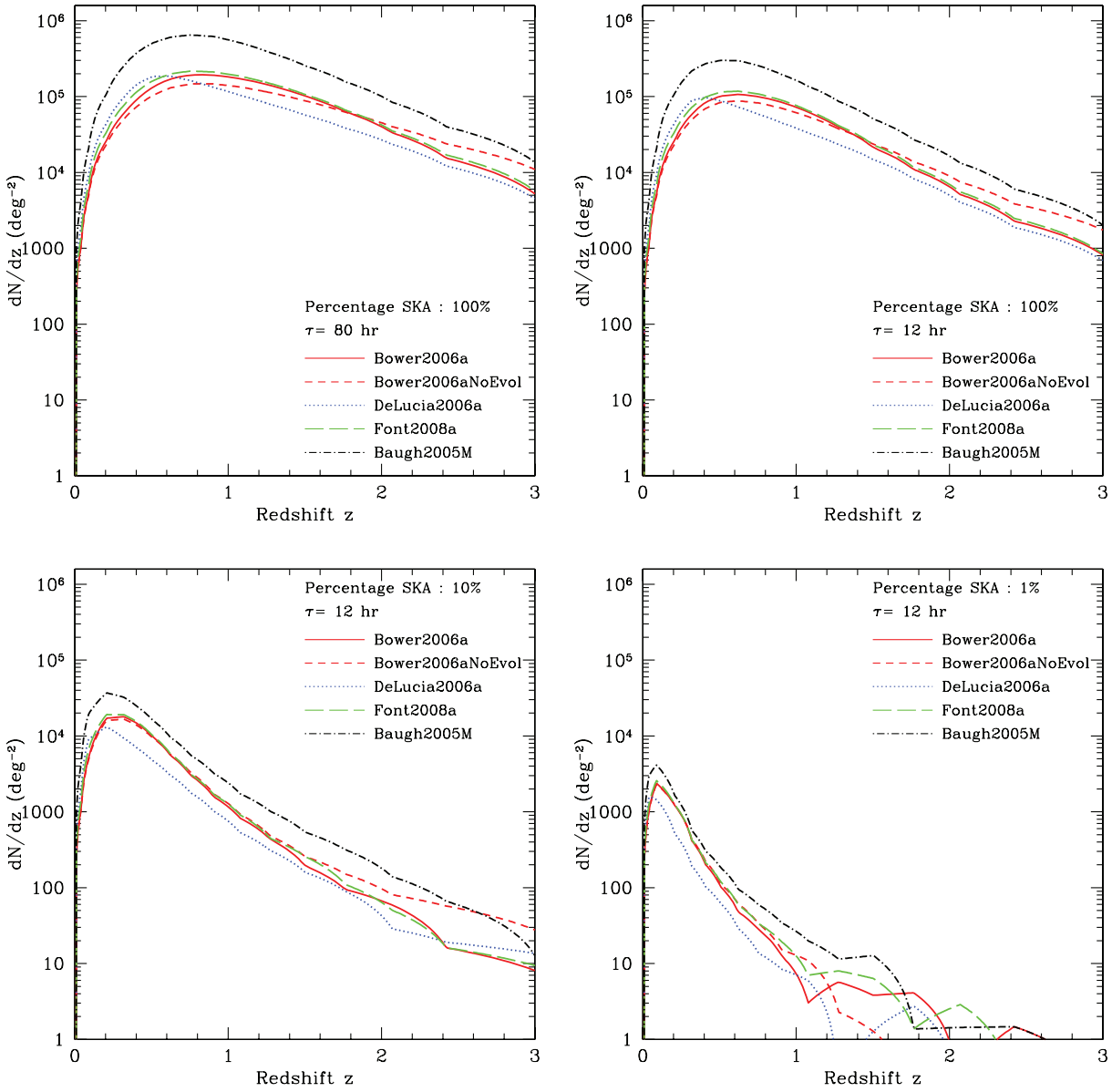


**Figure 7.** Number counts of galaxies per square degree per unit redshift for a telescope with 100 per cent (top left and right), 10 per cent (bottom left) and 1 per cent (bottom right) of the effective area of a fiducial SKA ($A_{\rm eff} = 1\,{\rm km}^2$), for a deep peak flux limited hemispheric H I survey lasting 1 yr. We consider two integration times; $\tau = 12$ h, appropriate for a field of view of 30 deg$^2$, which is typical of pathfinders such as ASKAP and MeerKAT, and $\tau = 80$ h, appropriate for a field of view of 200 deg$^2$, which is the maximum field of view anticipated for the full SKA. Only sources that satisfy $S_{\rm obs} \geq n_\sigma S_{\rm rms}$ with $n_\sigma = 10$ are included. Note that we do not include galaxies with cold gas masses below the resolution limit of $M_{\rm cold} = 10^{8.5}\,h^{-1}\,{\rm M}_\odot$. In all of the panels, we show how the counts change in Bower2006a if we assume a 'No Evolution' case in which the mass function predicted for $z = 0$ applies at all redshifts.

($A_{\rm eff} = 1\,{\rm km}^2$). $A_{\rm eff}$ is crucial in determining how many galaxies can be detected and the range of redshifts that can be probed. We find the number counts peak at $\sim 4 \times 10^3/4 \times 10^4/3 \times 10^5$ galaxies deg$^{-2}$ at $z \sim 0.1/0.2/0.5$ for an year long H I hemispheric survey on a 1/10/100 per cent SKA with a 30 deg$^2$ field of view, corresponding to an integration time of 12 h. On a full SKA with a 200 deg$^2$ field of view (equivalent to an integration time of 80 h), the number counts peak at $5 \times 10^5$ galaxies deg$^2$ at $z \sim 0.6$.

A couple of interesting trends are immediately apparent in this figure. The first is that DeLucia2006a, Bower2006a and Font2008a, which all incorporate a form of AGN feedback, all predict broadly similar number counts out to $z \sim 3$. There are differences in the details that reflect differences between the models that can be readily inferred from the mass functions shown in Fig. 1. For example, DeLucia2006a predicts enhanced number counts at lower redshifts and depressed number counts at intermediate to high redshifts with respect to Bower2006a and Font2008a. Here, lower, intermediate and higher are defined relative to the redshift at which the number counts peak – approximately $z \sim 0.5$, 1.0 and 1.5 for 1, 10 and 100 per cent of the effective area of the SKA, respectively. The second is that Baugh2005M consistently predicts many more gas-rich galaxies than the other three models. There are several reasons for this: (i) Baugh2005M incorporates galactic super winds rather than AGN feedback, which affects the cooling rate in massive haloes; (ii) it uses weaker supernovae feedback than the other models; and (iii) the star formation time-scale in galactic discs does not scale

with the disc dynamical time in Baugh2005M, whereas it does in the other models.

So far we have neglected the important issue of completeness of the number counts. As explained in Section 3, the finite mass resolution of the Millennium simulation implies that there is a minimum cold gas mass – and therefore a minimum H I mass – that can be reliably resolved in the Millennium galaxy formation models. For our assumed cold gas mass limit of $10^{8.5}\,M_\odot$, this implies a H I mass limit of $\sim 10^{8.2} M_\odot$ (assuming a fixed $H_2/H\,I$ approach to converting from cold gas mass to H I mass). The sensitivity of a survey may be such that galaxies with H I masses below this lower mass limit can be detected, and so we expect that the number counts of H I sources will be underestimated below some redshift $z_{\rm inc}$. This is because the cold gas mass function has not converged at low masses and so the population of sources is incomplete. As the sensitivity of a survey increases, so too does $z_{\rm inc}$ because the survey probes the H I mass function down to lower masses and the effect of this incompleteness will be in evidence at higher redshifts.

We have assessed the issue of completeness for one of the Durham models (Bower2006a) using three sets of merger trees of increasing resolution (1, 2 and 4 times the Millennium galaxy formation model resolution; MC1, MC2 and MC3, respectively) generated using the Monte Carlo prescription described in Section 3. We considered surveys with effective areas of 1/10/100 per cent of the SKA and integration times of 12 and 80 h. As we would expect, the number counts predicted using the $N$-body merger trees and the MC1 merger trees are consistent with one another; reassuringly, the same holds true for the MC2 and MC3 merger trees, for all of the survey sensitivities that we considered. This suggests that the number counts we obtain for Bower2006a with the $N$-body trees are converged and the peak redshifts and number counts we find in Fig. 7 are robust. We have also estimated the redshifts at which the limiting survey sensitivity (and consequently minimum H I mass detectable; see equation 11) is comparable to the limiting H I mass and we find that $z_{\rm inc} \lesssim 0.04$ for a 1/10 per cent SKA, and $z_{\rm inc} \simeq 0.08$ for a 100 per cent SKA. These estimates confirm that incompleteness effects are unlikely to affect the shape and amplitude of the peak of the number counts shown in Fig. 7 for Bower2006a.[8]

Fig. 7 is based on the fixed $H_2/H\,I$ approach to estimating H I masses from cold gas masses, but it is interesting to ask how the number counts would change if we used the variable $H_2/H\,I$ approach instead. In Fig. 8 , we compare the number counts of sources in Bower2006a estimated using the fixed $H_2/H\,I$ approach (solid curves) and the variable $H_2/H\,I$ approach (dashed curves). In the upper panel, we show the case for a 100 per cent SKA with an integration time of $\tau = 80$ h and in the lower panel we show the result for a 1 per cent SKA with an integration time of $\tau = 12$ h. As discussed in Section 4.1, we expect the number of sources to be systematically lower at higher redshifts if we adopt a variable rather than a fixed $H_2/H\,I$ ratio and this is confirmed by Fig. 8. The peak number of sources is lower in the variable approach and the number counts decline more sharply with increasing redshift. The difference is a factor of 10 for the 100 per cent (1 per cent) of the SKA by $z = 3$ (1).

[8] It is worth remarking that the precise value of $z_{\rm inc}$ will vary from model to model because each model predicts slightly different shapes for the H I mass function with decreasing mass, and so we should repeat this exercise for each model in principle. However, the consistency of Bower2006a with the other models suggests that conclusions about completeness based on this model are sufficiently general to be applied to the other models.

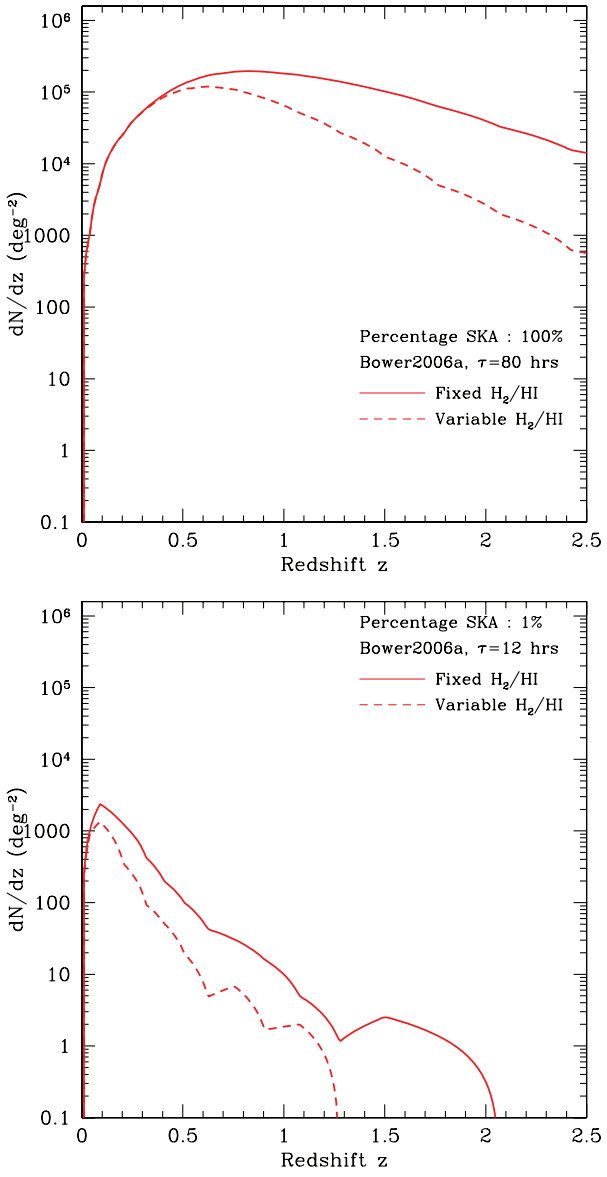


**Figure 8.** Number counts of galaxies per square degree per unit redshift for a telescope with 100 per cent (top panel) and 1 per cent (bottom panel) of the effective area of a fiducial SKA (1 km$^2$), for a peak flux limited H I survey lasting 1 yr, based on Bower2006a. The integration times are $\tau = 80$ and 12 h, respectively. As before, only sources that satisfy $S_{\rm obs} \geq n_\sigma S_{\rm rms}$ with $n_\sigma = 10$ are included and we ignore galaxies with cold gas masses below the resolution limit. The solid and dashed curves correspond to the (fiducial) fixed $H_2/H\,I$ and variable $H_2/H\,I$ approaches to estimating the cold gas mass to H I mass conversion factor.

In Fig. 1, we noted that the cold gas mass function does not appear to evolve strongly with redshift between $0 \leq z \lesssim 1$. It is therefore interesting to ask how approximating the mass function at $z$ by the mass function predicted at $z = 0$ impacts on the number counts of sources. In each of the panels in Fig. 7, the solid short dashed curves highlight the impact making such an approximation – showing the behaviour of the Bower2006a NoEvol approximation, in which the H I mass function at a given $z$ is replaced by the H I mass function predicted by Bower2006a at $z = 0$. For the 10 and 100 per cent SKA, this would appear to be a reasonable approximation over the redshift range $0 \lesssim z \lesssim 1.5$, differing by $\sim$10 per cent at most.

At $z \gtrsim 1.5$, the predicted number counts diverge the degree of the discrepancy depending on the sensitivity of the survey.

It is useful to compare our results with previous work, and so we note that Abdalla & Rawlings (2005) have predicted the redshift variation of $dN/dz$ for a full SKA using semi-empirical models for the H I mass function. This is interesting because we can compare predictions based on semi-analytical models with their predictions based on semi-empirical models. For a survey with an integration time of 4 h on a full SKA, they expect to detect $\sim 8 \times 10^4$ sources at the peak $dN/dz$; this peak occurs at $z \sim 0.6$. Based on a similar integration time, the semi-analytical models predict peak $dN/dz$s of between $\sim 8 \times 10^4$ (Bower2006a; DeLucia2006a; Font2008) and $\sim 2 \times 10^5$ (Baugh2005M). All of these models peak at $z \sim 0.5$. The semi-analytical models predict $dN/dz$s that decline more gently with increasing $z$ than the semi-empirical models but this reflects in part differences in the model assumptions (e.g. the assumption that H I, baryons and dark matter follow similar mass functions) and in part the conversion from cold gas to H I mass that we must assume.

Secondly, we focus on the angular sizes of galaxies. Figs 9 and 10 show how the angular size of H I galaxies varies with redshift. We compute the angular diameter as $\theta = 2\,R_{\rm h}/D_{\rm ang}$ where $R_{\rm h}$ is the half-mass radius of the galaxy and $D_{\rm ang}(z) = (1+z)^{-1}\,D_{\rm co}(z)$ is the angular diameter distance of the galaxy with respect to the observer, where, as before, $D_{\rm co}(z)$ is the radial comoving separation between source and observer. The points correspond to the median angular diameters while the upper and lower error bars indicate the 25th and 75th percentiles of the angular diameter distributions at that redshift. Points are given horizontal offsets of 0.025 in redshift to aid clarity. In Fig. 9, we plot the redshift dependence of the median angular diameters of galaxies with H I masses $M_{\rm H\,I} \geq 10^9\,h^{-1}\,{\rm M}_\odot$ (upper panel) and $M_{\rm H\,I} \geq 10^{10}\,h^{-1}\,{\rm M}_\odot$ (lower panel) varies with redshift out to $z \lesssim 3$. In Fig. 10, we focus on the variation predicted by Baugh2005 and DeLucia2006a for galaxies with $M_{\rm H\,I} \geq 10^9\,h^{-1}\,{\rm M}_\odot$ over the redshift interval $0 \leq z \leq 1$.

Knowledge of the expected redshift variation of angular diameter of an extended H I source is useful because it allows one to estimate the number of sources that are likely to be resolved out. Figs 9 and 10 distil the information presented in Fig. 4, where we showed how the half-mass radii of galaxies varied with cold gas mass at a given redshift. The models indicate that galaxies that have larger H I masses tend to have larger half-mass radii, which corresponds to more extended angular diameters at a given redshift. The angular diameter decreases sharply between $z = 0$ and $\simeq 0.5$, and more gently at $z \gtrsim 0.5$. The median angular size varies between 5 and 10 arcsec at $z = 0.1$, 1 and 3 arcsec at $z = 1$ and 1 and 3 arcsec at $z = 3$ for galaxies with H I masses in excess of $10^9\,h^{-1}\,{\rm M}_\odot$; the upper and lower bounds correspond to the predictions from DeLucia2006a and Baugh2005M. Therefore, to resolve a typical galaxy with an H I mass of $M_{\rm H\,I} \gtrsim 10^9\,h^{-1}\,{\rm M}_\odot$ at $z \sim 1$ requires a maximum baseline of the order of 100 km.

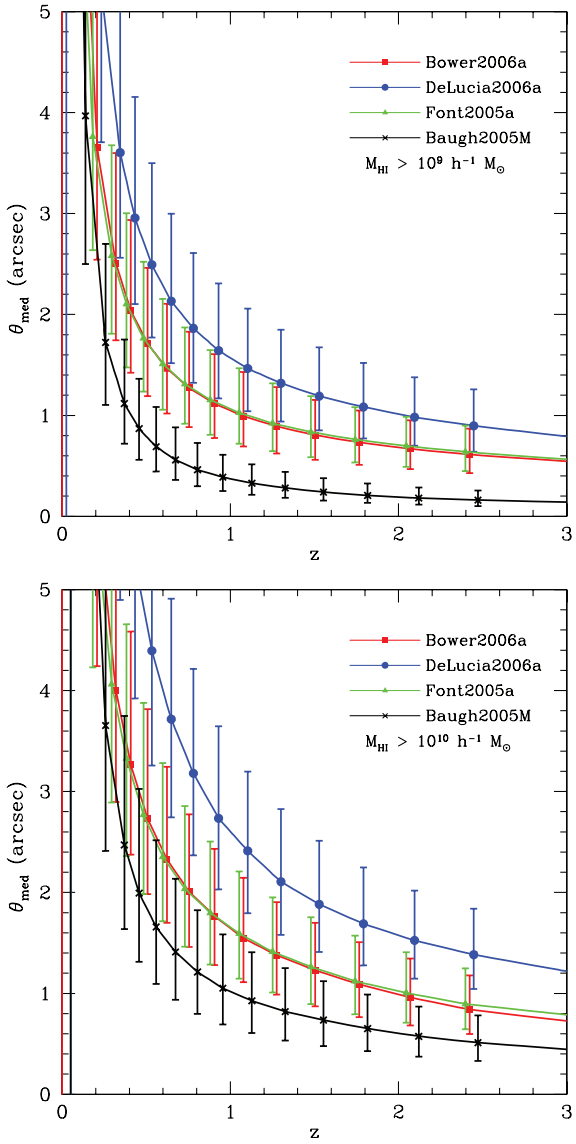


**Figure 9.** The predicted redshift variation of the angular diameter of galaxies with H I masses $M_{\rm H\,I} \gtrsim 10^9\,h^{-1}\,{\rm M}_\odot$ (upper panel) and $M_{\rm H\,I} \gtrsim 10^{10}\,h^{-1}\,{\rm M}_\odot$ (lower panel). Different symbols correspond to different models, as indicated by the legend.

## 5 SUMMARY

Neutral atomic hydrogen is the fundamental baryonic building block of galaxies and understanding how its abundance varies over cosmic time will provide us with important insights into galaxy formation. Few observational data exist for the abundance of neutral hydrogen at redshifts $z \gtrsim 0.05$, the extent of the HIPASS survey (Meyer et al. 2004), but this will change with the advent of the SKA, which will see first light by about 2020. The SKA will transform cosmology and galaxy formation (e.g. Blake et al. 2004; Braun 2007), allowing us to probe the cosmic H I distribution out to redshifts $z \sim 3$. In the meantime, H I surveys on SKA pathfinders such as ASKAP (Johnston et al. 2008), MeerKAT (Booth et al. 2009) and APERTIF (Verheijen et al. 2008) will provide us with important initial glimpses into the cosmic H I distribution out to redshifts $z \sim 1$. Because we have such few observational data for the cosmic H I distribution beyond $z \sim 0.05$, the coming decade promises to provide powerful tests of the predictions of theoretical galaxy formation models. It is therefore timely to ask what galaxy formation models tell us about the abundance of neutral hydrogen in galaxies.

In this paper, we have investigated four of the currently favoured galaxy formation models – those of Baugh2005M, Bower2006a, DeLucia2006a and Font2008a – and determined what they predict for the mass function of cold gas in galaxies and how it evolves with redshift. Each of the models use merger trees derived from the Millennium simulation (cf. Springel et al. 2005) and so any differences between the model predictions reflect intrinsic differences in the physics incorporated into the models themselves. Three of

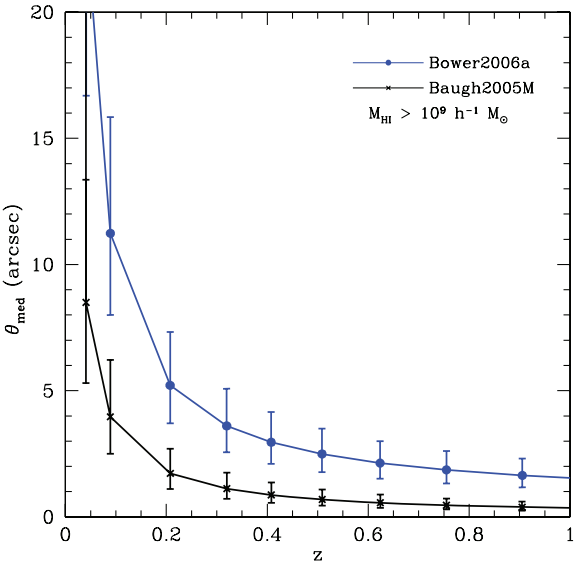


**Figure 10.** The predicted redshift variation of the angular diameter of galaxies with H I masses $M_{\rm H\,I} \gtrsim 10^9\,h^{-1}\,{\rm M}_\odot$ at $z \lesssim 1$ in Baugh2005M and DeLucia2006a.

the models (Baugh2005M, Bower2006a and Font2008a) use the Durham semi-analytical code GALFORM (cf. Cole et al. 2000) whereas the fourth (DeLucia2006a) uses the Munich semi-analytical code. Arguably, the most important difference between the models is in the precise treatment of feedback; Bower2006a, DeLucia2006a and Font2008a all incorporate a form of AGN feedback whereas Baugh2005M does not, instead favouring galactic super winds.

Interestingly, we find that the model predictions are broadly consistent with one another. Differences between the models reflect (i) the use of AGN heating to suppress gas cooling in massive haloes (which is used in Bower2006a, Font2008a and DeLucia2006a but not in Baugh2005M, which invokes supernovae-driven super winds); (ii) the strength of supernovae feedback, which is weakest in Baugh2005M; and (iii) the scaling (or lack of) of the star formation time-scale in galactic discs with the disc dynamical time (scaling is assumed in Bower2006a, DeLucia2006a and Font2008a whereas it is not in Baugh2005M).

We have focused on three particular aspects of the cold gas properties of galaxies, namely (i) the mass function of cold gas in galaxies and the relationship between (ii) a galaxy's cold gas mass and its half-mass radius and (iii) its cold gas mass and rotation speed (i.e. circular velocity) at this radius. The key results can be summarized as follows:

The predictions of Font2008a and Bower2006a are generally very similar, with differences only apparent at small cold gas masses. This is unsurprising because Font2008a descends directly from Bower2006a, the principal difference between the models being the improved treatment of gas stripping by the hot intracluster medium in Font2008a. At $z = 0$, we find that Bower2006 and Font2008 systematically overpredict the numbers of galaxies with H I masses in excess of $10^9\,h^{-2}\,{\rm M}_\odot$ when compared to the observed mass function derived from HIPASS (cf. Zwaan et al. 2005), while Baugh2005M and DeLucia2006a provide reasonable descriptions (i.e. in terms of shape and amplitude) of the observed mass function. Interestingly, we find that the cold gas mass function shows little evolution out to redshifts of $z \simeq 3$ in all four models.

At fixed cold gas mass, both Bower2006a and Font2008a predict half-mass radii and rotation speeds (circular velocities measured at these half-mass radii) that are in excellent agreement with each other, as we might expect. Half-mass radii are slightly but systematically larger (by ∼25 per cent) in DeLucia2006a than in Bower2006a and Font2008a, but the three models predict similar rotation speeds (to within the width of the distribution). This level of agreement is remarkable, given the number of subtle (and some not so subtle) differences between the frameworks underpinning DeLucia2006a and Bower2006a/Font2008a (described in Section 2). In contrast, Baugh2005M predicts half-mass radii that are systematically smaller (∼60 per cent) and rotation speeds that are systematically larger (by ∼20 per cent) at fixed cold gas mass than in Bower2006a, DeLucia2006a and Font2008a. It is worth noting that Baugh2005M predicts a size–luminosity relation for late-type galaxies that is in very good agreement with SDSS data, whereas the agreement between Bower2006a (and by extension Font2008a) and the observational data are poor (cf. Gonzalez et al. 2009).

We took the predicted mass functions of cold gas in galaxies and used them to derive number counts of H I galaxies for future all-sky H I surveys. Rather than adopting a specific design, we considered surveys carried out on radio telescopes with effective collecting areas $A_{\rm eff}$ that are percentages of a fiducial SKA, with an effective collecting area of $1\,{\rm km}^2$. We focused on surveys with $A_{\rm eff}$ of 1, 10 and 100 per cent of the SKA and assumed that these surveys lasted for 1 yr, with integration times of between 12 and 80 h within individual fields of view. As we pointed out in Section 4.2.1, $A_{\rm eff}$ plays a crucial role in determining the sensitivity $S_{\rm rms}$ of a radio telescope, which in turn dictates how many H I galaxies are likely to be detectable by the survey. SKA pathfinders such as ASKAP, MeerKAT and APERTIF will have effective areas of the order of ∼1 per cent.

We examined two possible approaches to converting cold gas masses to H I masses. The first simply assumed that the ratio of molecular-to-atomic hydrogen ($H_2$/H I) is fixed for all galaxies at all redshifts (cf. Baugh et al. 2004). The second assumed that the $H_2$/H I ratio is variable, depending on individual galaxy properties according to the model of Obreschkow et al. (2009a), which in turn is based on an empirical relation between the ratio of the surface densities of $H_2$ to H I and the gas pressure found for local galaxies by Blitz & Rosolowsky (2006) and Leroy et al. (2008). This is an important consideration because how one converts from cold gas mass to H I mass will determine the 21 cm luminosity of a galaxy and therefore its detectability in an H I survey of a given sensitivity. We computed the observed flux $S_{\rm obs}$ for each galaxy using both its H I mass and its circular velocity at the half-mass radius to define its velocity width and required that $S_{\rm obs} \geq 10 S_{\rm rms}$ for the galaxy to be detected.

As for the cold gas mass functions, we find that the models that include a form of AGN feedback predict broadly similar number counts; Baugh2005M predicts many more gas rich galaxies, as many as a factor of ∼2–3 more at the redshift at which the number counts peak. The choice of cold gas to H I mass conversion factor is also very important, especially at higher redshifts; adopting a variable $H_2$/H I ratio predicts that galaxies should be predominantly molecular rather than atomic hydrogen at high redshifts, and this has a profound impact on the number of H I sources one predicts (see Fig. 8). Clearly, more work is needed to put this on a more secure theoretical footing. Interestingly, we find that approximating the H I mass function at $z \lesssim 2$ by the $z = 0$ H I mass function has little impact on the number counts one might expect to measure.

In addition, we estimated the dependence of the median angular diameter of H I galaxies on redshift, for galaxies with H I masses

$M_{\rm HI} \geq 10^9\,h^{-1}\,{\rm M}_\odot$ and $M_{\rm HI} \geq 10^{10}\,h^{-1}\,{\rm M}_\odot$. This is useful to know because it allows one to estimate the fraction of the flux that is likely to be lost because it has been resolved out. The models indicate that galaxies with larger H I masses tend to have larger half-mass radii and therefore more extended angular diameters at a given redshift. We found that the angular diameter decreases sharply between $0 \lesssim z \lesssim 0.5$ and more gently at $z \gtrsim 0.5$. The median angular size varies between 5 and 10 arcsec at $z = 0.1$, 0.5 and 3 arcsec at $z = 1$ and 0.2 and 1 arcsec at $z = 3$ for galaxies with H I masses in excess of $10^9\,h^{-1}\,{\rm M}_\odot$, where the lower and upper limits correspond to the predictions of Baugh2005M and DeLucia2006a.

We have concentrated on the most straightforward measurement one can make in future H I surveys, namely the number counts of galaxies. However, we have considered only global counts – we have not considered how the H I mass functions and number counts might depend on local environment. Certainly, there is good reason to expect that environment should play a role in shaping the H I mass function of galaxies. For example, we might expect that the amount of H I in a galaxy will be reduced by ram-pressure stripping as it falls through a dense intracluster medium; this would become apparent as a quenching of the star formation (e.g. Balogh, Navarro & Morris 2000; Quilis, Moore & Bower 2000), but it should also be evident in an environmental dependence of a galaxy's H I properties. Indeed, there is some observational evidence to suggest that the H I mass function does depend on environment (e.g. Zwaan et al. 2005; Springob, Haynes & Giovanelli 2005; Kilborn et al. 2009); for example, Kilborn et al. (2009) find evidence that the slope of the low-mass end of the H I mass function in galaxy groups decreases with decreasing H I mass, in contrast to the global H I mass function found in HIPASS by Zwaan et al. (2005).

These results are interesting because they suggest that environment plays an important role in determining the H I properties of galaxies. In forthcoming papers, we will explore precisely what galaxy formation models predict for the clustering of cold gas (Kim et al. 2010) and we will explore precisely what role environment plays in shaping a galaxy's cold gas – and consequently H I – properties.

## ACKNOWLEDGMENTS

We thank the anonymous referee for their very helpful comments. CP thanks Chris Blake, John Helly and Lister Staveley-Smith for instructive discussions at various stages during the writing of this paper. This work was supported by separate STFC rolling grants at Leicester and Durham. CP acknowledges the support of the Australian Research Council funded 'Commonwealth Cosmology Initiative', DP Grant No. 0665574 during the initial stages of this work. We acknowledge the efforts of Andrew Benson, Richard Bower, Shaun Cole, Carlos Frenk, John Helly and Rowena Malbon in developing the GALFORM code used in the Baugh2005M model. This project was made possible by the availability of models on the Millennium archive set up the Virgo Consortium with the support of the German Astrophysical Virtual Observatory.

## REFERENCES

Abdalla F. B. Rawlings S., 2005, MNRAS, 360, 27
Abdalla F. B., Blake C. Rawlings S., 2010, MNRAS, 401, 743
Almeida C., Baugh C. M., Lacey C. G., 2007, MNRAS, 376, 1711
Almeida C., Baugh C. M., Wake D. A., Lacey C. G., Benson A. J., Bower R. G. Pimbblet K., 2008, MNRAS, 386, 2145
Balogh M. L., Navarro J. F., Morris S. L., 2000, ApJ, 540, 113
Baugh C. M., 2006, Rep. Prog. Phys., 69, 3101
Baugh C. M., Lacey C. G., Frenk C. S., Benson A. J., Cole S., Granato G. L., Silva L., Bressan A., 2004, New Astron. Rev., 48, 1239
Baugh C. M., Lacey C. G., Frenk C. S., Granato G. L., Silva L., Bressan A., Benson A. J., Cole S., 2005, MNRAS, 356, 1191 (Baugh2005M)
Benson A. J., Bower R. G., Frenk C. S., Lacey C. G., Baugh C. M., Cole S., 2003, ApJ, 599, 38
Blake C. A., Abdalla F. B., Bridle S. L., Rawlings S., 2004, New Astron. Rev., 48, 1063
Blitz L., Rosolowsky E., 2006, ApJ, 650, 933
Booth R. S., de Blok W. J. G., Jonas J. L., Fanaroff B., 2009, preprint (arXiv:0910.2935)
Bower R. G., Benson A. J., Malbon R., Helly J. C., Frenk C. S., Baugh C. M., Cole S., Lacey C. G., 2006, MNRAS, 370, 645 (Bower2006a)
Braun R., 2007, preprint (arXiv:astro-ph/0703746)
Burke B. F., Graham-Smith F., 1996, An Introduction to Radio Astronomy, Cambridge Univ. Press, Cambridge
Chengalur J. N., Braun R., Wieringa M., 2001, A&A, 372, 768
Cole S., Lacey C. G., Baugh C. M., Frenk C. S., 2000, MNRAS, 319, 168
Cole S. et al., 2001, MNRAS, 326, 255
Cole S., Helly J., Frenk C. S., Parkinson H., 2008, MNRAS, 383, 546
Croton D. J. et al., 2006, MNRAS, 365, 11
Davis M., Efstathiou G., Frenk C. S., White S. D. M., 1985, ApJ, 292, 371
De Lucia G., Blaizot J., 2007, MNRAS, 375, 2 (DeLucia2006a)
De Lucia G., Springel V., White S. D. M., Croton D., Kauffmann G., 2006, MNRAS, 366, 499
Drory N., Salvato M., Gabasch A., Bender R., Hopp U., Feulner G., Pannella M., 2005, ApJ, 619, L131
Elmegreen B. G., 1993, ApJ, 411, 170
Ferrière K. M., 2001, Rev. Mod. Phys., 73, 1031
Font A. S. et al., 2008, MNRAS, 389, 1619 (Font2008a)
Fontana A. et al., 2004, A&A, 424, 23
Giovanelli R. et al., 2005, AJ, 130, 2598
Gonzalez J. E., Lacey C. G., Baugh C. M., Frenk C. S., Benson A. J., 2009, MNRAS, 397, 1254
Gonzalez-Perez V., Baugh C. M., Lacey C. G., Almeida C., 2009, MNRAS, 398, 497
Harker G., Cole S., Helly J., Frenk C., Jenkins A., 2006, MNRAS, 367, 1039
Helly J. C., Cole S., Frenk C. S., Baugh C. M., Benson A., Lacey C., 2003, MNRAS, 338, 903
Hopkins A. M., 2004, ApJ, 615, 209
Jenkins A., Frenk C. S., White S. D. M., Colberg J. M., Cole S., Evrard A. E., Couchman H. M. P., Yoshida N., 2001, MNRAS, 321, 372
Johnston S. et al., 2008, Exp. Astron., 22, 151
Kennicutt R. C. Jr, 1998, ApJ, 498, 541
Keres D., Yun M. S., Young J. S., 2003, ApJ, 582, 659
Kilborn V. A., Forbes D. A., Barnes D. G., Koribalski B. S., Brough S., Kern K., 2009, MNRAS, 400, 1962
Kim H. S., Baugh C. M., Benson A. J., Cole S., Frenk C. S., Lacey C. G., Power C., Schneider M., 2010, MNRAS, submitted (arXiv:1003.0008)
Kitzbichler M. G., White S. D. M., 2007, MNRAS, 376, 2
Krumholz M. R., McKee C. F., Tumlinson J., 2009, ApJ, 693, 216
Lacey C. G., Baugh C. M., Frenk C. S., Silva L., Granato G. L., Bressan A., 2008, MNRAS 385, 1155
Lah P. et al., 2007, MNRAS, 376, 1357
Lah P. et al., 2009, MNRAS, 399, 1447
Leroy A. K., Walter F., Brinks E., Bigiel F., de Blok W. J. G., Madore B., Thornley, M. D., 2008, AJ, 136, 2782
Madau P., Ferguson H. C., Dickinson M. E., Giavalisco M., Steidel C. C., Fruchter A., 1996, MNRAS, 283, 1388
McCarthy I. G., Frenk C. S., Font A. S., Lacey C. G., Bower R. G., Mitchell N. L., Balogh M. L., Theuns T., 2008, MNRAS, 383, 593
Meyer M. J. et al., 2004, MNRAS, 350, 1195
Obreschkow D., Rawlings S., 2009, MNRAS, 394, 1857
Obreschkow D., Croton D., De Lucia G., Khochfar S., Rawlings S., 2009a, ApJ, 698, 1467

Obreschkow D., Heywood I., Klöckner H. -R., Rawlings S., 2009b, ApJ, 703, 1890
Parkinson H., Cole S., Helly J., 2008, MNRAS, 383, 557
Péroux C., McMahon R. G., Storrie-Lombardi L. J., Irwin M. J., 2003, MNRAS, 346, 1103
Prochaska J. X., Herbert-Fort S., Wolfe A. M., 2005, ApJ, 635, 123
Quilis V., Moore B., Bower R., 2000, Sci, 288, 1617
Rao S., Briggs F., 1993, ApJ, 419, 515
Rao S. M., Turnshek D. A., Nestor D. B., 2006, ApJ, 636, 610
Reynolds R. J., 2004, Adv. Space Res., 34, 1
Spitzer L., 1978, Physical Processes in the Interstellar Medium. Wiley-Interscience, New York
Springel V., White S. D. M., Tormen G., Kauffmann G., 2001, MNRAS, 328, 726
Springel V. et al., 2005, Nat, 435, 629
Springob C. M., Haynes M. P., Giovanelli R., 2005, ApJ, 621, 215
Taylor A. R., 2008, IAU Symp., 248, 164
Verheijen M. A. W., Oosterloo T. A., van Cappellen W. A., Bakker L., Ivashina M. V., van der Hulst J. M., 2008, in Minchin R., Momjian E., eds, AIP Conf. Ser. Vol. 1035, The Evolution of Galaxies Through the Neutral Hydrogen Window. Am. Inst. Phys., Melville, New York
Weinmann S. M., van den Bosch F. C., Yang X., Mo H. J., 2006a, MNRAS, 366, 2
Weinmann S. M., van den Bosch F. C., Yang X., Mo H. J., Croton D. J., Moore B., 2006b, MNRAS, 372, 1161
Wong T., Blitz L., 2002, ApJ, 569, 157
Zwaan M. A., 2000, PhD thesis, Rijksuniversiteit, Groningen
Zwaan M. A., Briggs F. H., Sprayberry D., Sorar E., 1997, ApJ, 490, 173
Zwaan M. A., Meyer M. J., Staveley-Smith L., Webster R. L., 2005, MNRAS, 359, L30

This paper has been typeset from a TEX/LATEX file prepared by the author.